nature portfolio

Peer Review File

Stronger ENSO-induced Global SST Variability in a Warming Climate

Corresponding Author: Professor Jong-Seong Kug

This file contains all reviewer reports in order by version, followed by all author rebuttals in order by version.

Version 0:

Reviewer comments:

Reviewer #1

(Remarks to the Author)
Review of the manuscript entitled "Stronger ENSO-induced Global SST Variability in a Warming Climate"

In this study, the authors explore how greenhouse warming modulates the influence of ENSO on global SST variability. They show that the ENSO-driven SST variability is expected to amplify in a warmer climate, primarily due to the increase in El Niño-induced surface wind speed anomaly and the climatological air-sea humidity difference. The study highlights that these changes arise from the strengthened ENSO teleconnections and overall warming of the global oceans, respectively. The findings provide important new insights into the mechanisms that could intensify regional climate impacts of future El Niño events. Overall, the manuscript is well-organized and presents several novel findings. I believe it could be suitable for publication after some major revisions. My specific comments are as follows:

Main comments:

1. Although this manuscript primarily focuses on the impact of unit-strength ENSO events on global SST variability, it is the overall influence of ENSO on the climate system that is of greater concern, particularly for policy-making and climate risk management. While the authors briefly discuss the effects of ENSO amplitude changes at the end of the manuscript, I suggest that they should present the total change in ENSO's influence on global SST and quantify the relative contributions of two factors: (a) changes in the sensitivity of SST to unit-strength ENSO events, and (b) changes in ENSO amplitude. Such an analysis would help determine whether the former plays the dominant role in amplifying ENSO's impact on SSTs. Recent studies (Lin et al. 2024; Wu et al. 2021) have employed a regression-based method to disentangle the contributions of ENSO amplitude changes and climate sensitivity to ENSO in shaping ENSO's influence on regional atmospheric circulation and SST variability. I recommend that the authors refer to these approaches and consider adopting a similar methodology.

2. The authors attribute the enhanced SST variability associated with ENSO primarily to the strengthening of surface flux anomalies, particularly latent heat flux (LHF). Based on qualitative analysis, they argue that the increase in global-mean LHF anomalies is driven by both enhanced climatological air-sea humidity differences and strengthened ENSO-induced surface wind anomalies. However, for several key regions, the analysis lacks sufficient quantitative support to convincingly identify the dominant physical drivers. Merely showing the spatial patterns of total LHF and wind anomalies is not adequate to substantiate the claim (Lines 201–203) that "the East CS, U.S. East Coast, and SNP are primarily attributed to anomalous wind variations, whereas the SIO is influenced by humidity changes." For instance, over the U.S. East Coast, the climatological specific humidity contrast (qs – qa) shows a substantial increase, which could potentially contribute more to the LHF anomalies than wind speed changes. Similarly, the changes in the SIO region may not be solely governed by the increase in anomalous humidity gradient. I therefore strongly recommend that the authors perform a more detailed quantitative analysis using the bulk formula for LHF to examine the contributions from changes in wind speed anomaly, climatological qs – qa, and ENSO-induced humidity gradient anomaly, and other relevant factors. The authors could refer to Lin et al. (2024) for relevant diagnostic approaches and analyses.

3. It is well known that El Niño and La Niña are asymmetric in terms of the center of SSTA, amplitude, persistence, and other characteristics, leading to their distinct and asymmetric impacts on the global climate. However, the current analysis is primarily based on correlation or regression methods, which implicitly assume linearity and overlook the influence of ENSO

asymmetry. Therefore, I think that the authors should examine the composite changes in global SST separately for El Niño and La Niña events. At the very least, they should acknowledge this limitation and provide a brief discussion of its potential implications for their results.

4. I noticed that the equatorial Indian Ocean exhibits a significant decrease in ENSO-induced SST variability. However, both surface wind speed and the climatological humidity gradient in this region are projected to strengthen under global warming, which suggests that changes in LHF anomalies alone may not fully explain the reduced SST variability there. Do the authors have a plausible explanation for this contrasting behavior? What mechanisms might be responsible for the weakened ENSO-induced SST variability in this region, especially given the overall strengthening of ENSO impacts observed elsewhere?

References:
Lin, S., B. Dong and S. Yang, 2024: Enhanced impacts of ENSO on the Southeast Asian summer monsoon under global warming and associated mechanisms. Geophysical Research Letters, 51, e2023GL106437. DOI: 10.1029/2023GL106437

Wu, M., Zhou, T., & Chen, X. (2021). The source of uncertainty in projecting the anomalous western North Pacific anticyclone during El Niño–decaying summers. Journal of Climate, 34(16), 6603–6617. https://doi.org/10.1175/JCLI-D-20-0904.1

Specific Comments:

Lines 40–42: Consider citing some references here to support the statement, such as recent studies on the enhanced impact of ENSO on East Asian climate under global warming (e.g., Lin et al. 2024).

Lines 57–59: I also suggest citing more recent literature to support this point.

Line 72: It is unclear whether this refers to a 3-month mean SSTA or a 3-month running mean SSTA. This should be clarified, as the method section (Line 281) seems to indicate the latter.

Lines 133–138 & Extended Data Fig. 4: It is difficult to conclude from this figure that the increased SFC are dominated by longwave radiation induced by ENSO. Please add the difference between the 2100 and PD to help support this claim.

Line 144: Consider changing “moisture anomalies” to “mean moisture,” if referring to the background state.

Lines 165–166: Do you mean the mean or the anomaly of the specific humidity difference (qs – qa)? I believe the intended meaning may be the change in the climatological humidity gradient. Please clarify.

Extended Data Fig. 5: The labels are too small, making the figure difficult to read. The authors may want to adjust the panel layout to enlarge each subplot and improve legibility.

Lines 186–203: The change in latent heat flux anomalies can result from variations in wind speed, climatological humidity gradient, or the anomalous humidity gradient. In particular, over the U.S. East Coast, the increase in the climatological humidity gradient is substantial, yet no quantitative evidence is provided, and only the conclusion that wind anomalies dominate is stated. I recommend that the authors conduct a quantitative decomposition using the bulk formula for LHF to support their interpretation. In addition, including a time series plot (similar to Fig. 4) that illustrates the evolution of LHF anomalies and their components (e.g., wind speed, qs – qa) during the development and decay phases of ENSO would help elucidate the physical processes for the reader.

Line 291: How do the authors calculate the SST tendency? Is it estimated based on the mixed-layer heat budget equation, or directly quantified using the time tendency of mixed-layer SST from model output? Please clarify this in the manuscript.

Line 300 & Figure 2: I am confused about the relationship between SSTSFC+MLD and SSTTOT. The integration of SFC from MAM to τ should correspond to the SST anomaly change from spring to τ, i.e., the difference between SSTTOT and SSTMAM. Therefore, in terms of magnitude, this difference may better correspond to the SSTSFC+MLD than SSTTOT alone.

Reviewer #2

(Remarks to the Author)
I co-reviewed this manuscript with one of the reviewers who provided the listed reports. This is part of the Nature Communications initiative to facilitate training in peer review and to provide appropriate recognition for Early Career Researchers who co-review manuscripts.

Reviewer #3

(Remarks to the Author)

It is very interesting to see the novel analysis to find the maximum variance of the SST response (maximum R2 value), taking into account the time lag "tau", and the distribution of the wind speed response at the time when the ENSO effect is maximized. The finding is also new that the amplitude of influence of ENSO on SSTs increases globally with global warming. On the other hand, the interpretation of the mechanism seems to me to leave some questions unanswered, and I feel that the understanding of the process is not fully developed. The details are described below, but given the number of questionable aspects of the process and the possibility that the way the logic is constructed may need to be fundamentally revised, I would recommend that the paper be rejected and resubmitted after sufficient time for revision.

Major points:
(1) The biggest question is that the pattern of wind speed response considering the lag "tau" remains the same whether it is EP or CP, and whether the ENSO amplitude is larger or smaller due to global warming (L220-L231, Fig. 3 and Extended Data Fig. 9). The only possible explanation for the agreement in those figures, even though the teleconnection patterns should clearly be different, is that the lag "tau" is different at each location. (Please show the spatial map of lag "tau" for EP and CP.) It seems to me that the process is no longer about the physics of the ENSO response, but we are simply seeing that the wind speed responses to any forcing from the tropics appears to deviate with large anomalies at the same location at the same timing “tau” that matches the location where the amplitude of the climatological wind speed variation is large. Please plot the spatial map of the annual maxima of wind speed variance on a global map and see if they are consistent with Fig. 3 and Extended Data Fig. 9.

(2) Regarding the similarity of the spatial pattern of the maximum R2 values in EP and in CP, it appears that the locations where the maximum R2 values are larger (Fig. 1 and Extended Data Fig. 8) correspond to locations where the climatological MLD is shallower (Extended Data Figure 3-a and b). It appears to me that this just means that the shallower the MLD is, the more sensitive it is to atmospheric Q_LH variation. Since the text only discusses the impact of MLD changes due to global warming, I believe that a logical connection is missing.

(3) The same is true for changes due to global warming: is it possible that the amplitude of the general atmospheric teleconnection to any forcing from the tropics is increasing, and the "increased amplitude of response associated with ENSO" referred to in this paper is only a part of what we are seeing?

If the above considerations (1) through (3) are true, then the logic construct and story structure of this paper, including the title, needs to be fundamentally revised. This will take time, which is why I have recommended a rejection and resubmission.

Requests for additional analyses:
(4) In the analysis of maximum R2 value, it is not clear which values are related each other and which are independent, so it would help to understand the mechanism if a map of the lag "tau" at the maximum absolute value is drawn together. In MME, is there uncertainty in the spatial distribution of the lag "tau"?

(5) In the analyses, MAM(0) is used as the baseline and the difference from it is analyzed to judge the maximum R2 value and conduct the mixed layer heat budget analysis. But the spatial distribution of the maximum R2 value or the heat budget terms must depend not only on the values at the time lag "tau" but also on the pattern at MAM(0). How much of impacts do this baseline values have?

(6) In the Eq.1, not only the SFC term but also the other budget terms (the advection terms, diffusion term) should be shown.

(7) To understand the differences among MME models in the maximum R2 values and wind speed responses, please add figures of the maximum R2 values and wind speed regressions for each model to the Extended Data Figures.

Minor comments
(8) L32-L42: Shifts in the position of the westerly jets due to global warming should also be important in changing the teleconnection pattern. Please add this in the text as it is an important factor in understanding the process of this study.

(9) L81-L82: Is the time lag "tau" also similar at each grid point between CESM1 LE and the observations?

(10) L90-L91: What are the reasons for the weakening of the ENSO impact in the tropical Indian Ocean?

(11) Please specify the number of ensembles in the CMIP6 1pctCO2 experiments for each model.

(12) L115: Before the explanation of "MLD", the subscript representation of "SFC+MLD" appears. At this point, there is no explanation of the difference between "SFC+MLD" subscripts, "SFC"-only subscripts, and "MLD"-only subscripts, which is confusing, so please revise the order of the explanations.

(13) L284: Why did you use MAM(0) as the baseline? Why were DJF(0) and JFA(0) skipped?

(14) L484 (Fig. 3 caption): "g" -> "d"

(15) L486 (Fig. 3 caption): "d-e" -> "e-f"

(16) L487 (Fig. 3 caption): "f" -> "g"

Reviewer #4

(Remarks to the Author)

The manuscript investigates the changes in ENSO-related SST variability under global warming based on climate models. It is a very interesting work suggesting that per-unit ENSO SST anomalies could induce amplified global-scale SST feedback responses under global warming scenarios. The results carry significant implications for improving climate projections of future variability. Through heat budget analysis using model data, the manuscript indicates that intensified ENSO-related wind speed and air-sea humidity difference are the main factors contributing to the enhanced SST anomaly responses. To address distinct climate regimes for different regions, the manuscript conducts diagnostics on four selected regions exhibiting specific atmospheric feedback responses.

The study is well designed and the manuscript is clearly written, guiding the reader towards its main conclusions. The methods section and the Extended file cover necessary details on datasets, analysis and experiments.

I guess my main comment/question lies in why could the same unit of ENSO SST anomalies lead to a stronger wind feedback through intensified atmospheric convection in the 2100 scenarios, compared with the PD simulation as showed in Figure.3. In other words, why could the same magnitude of ENSO SSTA induce stronger atmospheric convection feedback in a warming world? Is the cause attributed to changes in the atmospheric mean states affecting convective processes, an acceleration in atmosphere feedback establishment, or other factors? I guess a deeper analysis or discussion would greatly improve the comprehension of the underlying physical mechanisms in this manuscript.

Specific comments:
1) I suggest the manuscript could include some analyses on the changes in ENSO amplitude (PD .vs. 2100) from CESM1 runs. On this basis, the manuscript further examines the global SST variations induced by per unit amplitude of ENSO SSTA —even though this does not fundamentally alter the work's main conclusions.

2) Do any grid points exhibit τ values preceding the ENSO peak (e.g. Atlantic Niño (JJA0) could trigger an ENSO (D0JF1) event)? If present, would this phase-leading relationship necessitate larger-amplitude SSTA forcing to produce equivalent ENSO SST anomaly intensities?

3) According to Figure.1, the explainable variance R2 of SST in 2100 simulation is stronger than that in PD. Does this finding suggest a strengthening of the linear response component in ENSO's climatic impacts in 2100 due to more stable atmospheric stratification?

4) L33: Suggest using “anomalies” instead of “anomaly”.

5) There appears to be an inconsistency in Figure 3, where the annotations for panels (e) and (g) seem to be inadvertently swapped.

6) In Figure 4b-e, what does the hatches between the blue and red lines represent?

7) In Figure 4b-e, unlike the SST results, the temporal evolution of regression coefficients for latent heat flux appears to exhibit distinct peak timings (except SIO). Does this suggest an alteration in air-sea interaction processes between PD and 2100?

8) There are differences in the chosen time window for τ (L285: JJA(0)-JJA(1); L314: MAM(0)-JJA(1)) in Methods.

Version 1:

Reviewer comments:

Reviewer #1

(Remarks to the Author)
The authors have satisfactorily addressed all my previous concerns, and I recommend the manuscript for acceptance.

Reviewer #2

(Remarks to the Author)
I co-reviewed this manuscript with one of the reviewers who provided the listed reports. This is part of the Nature Communications initiative to facilitate training in peer review and to provide appropriate recognition for Early Career Researchers who co-review manuscripts.

Reviewer #3

(Remarks to the Author)
I sincerely appreciate the authors' conscientious and thoughtful responses. While I believe that many of the points have been addressed appropriately, I feel that the response regarding the part that I find most questionable—the understanding of the process—has not been explained sufficiently.

My main concern is that, regardless of whether the forcing originates from ENSO, CP, or EP, the maximum R2 pattern and the wind speed response appear quite similar. This suggests that the phenomenon may no longer be specific to ENSO. By focusing exclusively on ENSO, I am concerned that the authors may be overlooking a more fundamental and general process that does not depend on ENSO.

In Fig. R2-1, the authors state that the agreement between panels (a, b, c), and d is less than 20%; however, to my eye, the pattern correlations appear to be reasonably high. I do not think perfect coincidence is necessary, so I recommend examining the comparisons more carefully.

In the response to my Comment 2, the authors state that the pattern correlation between the climatological mixed layer depth (MLD) and the peak R2 was sufficiently small. However, are you not including the tropical Pacific in the correlation calculation? As the authors mentioned in another section, the auto-correlation in the tropical Pacific should be excluded from the analysis. Please check whether a significant negative correlation appears outside the tropical Pacific.

Would there not also be a meaningful correlation between the changes in MLD under global warming and the corresponding changes in peak R2? I encourage the authors to examine this relationship carefully.

In addition, please check whether the responses to tropical forcings in the Atlantic and Indian Ocean basins show similar behavior. I believe it is important to carefully consider whether the logical development of the paper should start specifically from ENSO, or rather from tropical forcing more broadly.

Reviewer #4

(Remarks to the Author)
I appreciate the authors' diligent effort in revising this manuscript and providing a point-by-point response. My previous major comments have been satisfactorily addressed. However, I guess a minor point need to be addressed to finalize the paper.

Previous Specific Comment #1:

I appreciate the significant effort and thoroughness in revising the manuscript. The addition of the quantitative decomposition analysis, separating the ENSO impact on global SST into non-amplitude and amplitude components, is a substantial and excellent improvement that greatly strengthens the rigor of your conclusions. However, the changes in ENSO amplitude remain unclear for the CESM1 and CMIP6 runs in this study. As the authors stated in the revised manuscript, ENSO amplitude changes should not be negligible, even though the non-amplitude component of ENSO plays a more significant role in influencing global SST.

Version 2:

Reviewer comments:

Reviewer #3

(Remarks to the Author)
I appreciate the authors' careful consideration of my comments. The authors have now explicitly discussed the influence of other ocean basins in the Discussion section, and I think this largely addresses my concerns. I have only one minor comment.
In Supplementary Fig. 17, the use of partial linear regression is not fair, because it removes all variability in the Indian and Atlantic Oceans that covaries with ENSO. For a fair comparison, either (1) Supp. Fig. 17b and c should also use standard (non-partial) regression, or (2) the influences of the Indian and Atlantic Oceans should be removed from the ENSO analysis in Supp. Fig. 17a (and similarly, the influences of ENSO and the Atlantic Ocean should be removed from the Indian Ocean analysis, and likewise for the Atlantic Ocean).
If this point is revised, I believe the manuscript would be suitable for acceptance.

Reviewer #4

(Remarks to the Author)
The authors have properly addressed my comments, and the revised manuscript is acceptable for publication.

Response to Reviewer #1

In this study, the authors explore how greenhouse warming modulates the influence of ENSO on global SST variability. They show that the ENSO-driven SST variability is expected to amplify in a warmer climate, primarily due to the increase in El Niño-induced surface wind speed anomaly and the climatological air-sea humidity difference. The study highlights that these changes arise from the strengthened ENSO teleconnections and overall warming of the global oceans, respectively. The findings provide important new insights into the mechanisms that could intensify regional climate impacts of future El Niño events. Overall, the manuscript is well-organized and presents several novel findings. I believe it could be suitable for publication after some major revisions.

We thank the reviewer for the encouraging and constructive comments. The comments were fully considered in the revised manuscript. The point-by-point responses are as follows:

Comments:

1. Although this manuscript primarily focuses on the impact of unit-strength ENSO events on global SST variability, it is the overall influence of ENSO on the climate system that is of greater concern, particularly for policy-making and climate risk management. While the authors briefly discuss the effects of ENSO amplitude changes at the end of the manuscript, I suggest that they should present the total change in ENSO's influence on global SST and quantify the relative contributions of two factors: (a) changes in the sensitivity of SST to unit-strength ENSO events, and (b) changes in ENSO amplitude. Such an analysis would help determine whether the former plays the dominant role in amplifying ENSO's impact on SSTs. Recent studies (Lin et al. 2024; Wu et al. 2021) have employed a regression-based method to disentangle the contributions of ENSO amplitude changes and climate sensitivity to ENSO in shaping ENSO's influence on regional atmospheric circulation and SST variability. I recommend that the authors refer to these approaches and consider adopting a similar methodology.

Ans) We appreciate this insightful suggestion and fully agree that assessing ENSO's total influence on SST is also crucial. In the revision, we quantified ENSO's overall impact on SST as the product of (i) the sensitivity of SST to a unit-strength ENSO event (the regression coefficient, β) and (ii) ENSO amplitude (the standard deviation of the ENSO index, σ). Following the regression-based decompositions used by Lin et al. (2024) and Wu et al. (2021), we expressed the projected change in ENSO's SST influence (Δ[βσ]) as the sum of a "non-amplitude" term (σ·Δβ), an "amplitude" term (β·Δσ), and a small second-order residual (Δβ·Δσ). We had added this method to the Extended Data Text.

Decomposition of changes in El Niño impacts on SSTA

The changes in El Niño impacts on SST is calculated as follows:

$$Y' = \beta \times \text{Niño3.4} + Res_1, \qquad (S1)$$

where Y' is SSTA(τ), β is the regression coefficient, which indicates ENSO-induced SSTA, and Res_1 is the residual. Unit of β is K per 1K of DJF Niño3.4 SSTA (DJF Niño3.4). We used the $|\beta|$ as a representation of ENSO impacts on SSTA.

Following the Lin et al. (2024) and Wu et al. (2021), SSTA(τ) regression is also conducted with DJF Niño3.4$_{std}$, which represent standardized Niño3.4 SSTA as follows:

$$\text{Niño3.4}_{std} = \text{Niño3.4}/\sigma$$
$$Y' = \beta_{std} \times \text{Niño3.4}_{std} + Res_2, \qquad (S2)$$

where σ is the standard deviation of DJF Niño3.4, β_{std} is the regression coefficient indicating ENSO-induced SSTA per one standard deviation of ENSO, and Res_2 is the residual. β_{std} consists of two influences: (i) non-amplitude factor (the regression coefficient, β) and (ii) ENSO amplitude factor (the standard deviation of the ENSO index, σ). Since the $|\beta_{std}| \approx |\beta| \times \sigma$ from Eq. S2 and S3, the decomposition of these two factors is calculated as follows:

$$\Delta|\beta_{std}| = \Delta|\beta| \times \sigma_{PD} + |\beta_{PD}| \times \Delta\sigma + Res_3, \qquad (S3)$$

where Δ means difference between 2100 and PD periods, the subscript PD indicates the PD period, Res_3 is the residual term. Using Eqs. S2 and S3, we decompose the contributions of non-amplitude and amplitude factor.

Applying this framework, we found that in CESM1 the increase in ENSO's SST influence is explained primarily by the non-amplitude component (~64%), with a smaller but non-negligible contribution from amplitude changes (~32%); the remainder is a small cross term. In the CMIP6 multi-model mean, the dominance of the non-amplitude component is even clearer (~76%), whereas amplitude changes account for ~20%, with a small residual term.

These results indicate that background state- and teleconnection-related changes in SST sensitivity to a unit ENSO amplitude play a leading role in amplifying ENSO's overall SST impact, consistent with our main finding that strengthened El Niño-induced wind-speed anomalies and enhanced climatological air-sea humidity contrast drive the projected amplification. The relatively modest contribution of the amplitude factor in the CMIP6 mean also aligns with the interpretation of Extended Data Figure 15.

We have revised the Discussion section and added a new Extended Data Figure 14 that maps the total change and its decomposition (non-amplitude vs amplitude).

(L237-245): To quantify ENSO's total SST influence, we decomposed it into a non-amplitude term and an amplitude term, following regression-based approaches (Extended Data Text). The results show that the increase is dominated by non-amplitude component changes—~64% in CESM1 and ~76% in the CMIP6 multi-model mean—while amplitude accounts for ~32% and ~20%, respectively; importantly, even models with reduced ENSO amplitude[54–56] show a net increase because atmospheric and oceanic sensitivity strengthens (Extended Data Fig. 15 and 16). In summary, background-state/teleconnection changes dominate, but amplitude changes are not negligible.

Lin, S., Dong, B. & Yang, S. Enhanced Impacts of ENSO on the Southeast Asian Summer Monsoon Under Global Warming and Associated Mechanisms. Geophysical Research Letters 51, e2023GL106437 (2024).

Wu, R., Chen, W., Wang, G. & Hu, K. Relative contribution of ENSO and East Asian winter monsoon to the South China Sea SST anomalies during ENSO decaying years. Journal of Geophysical Research: Atmospheres 119, 5046–5064 (2014).

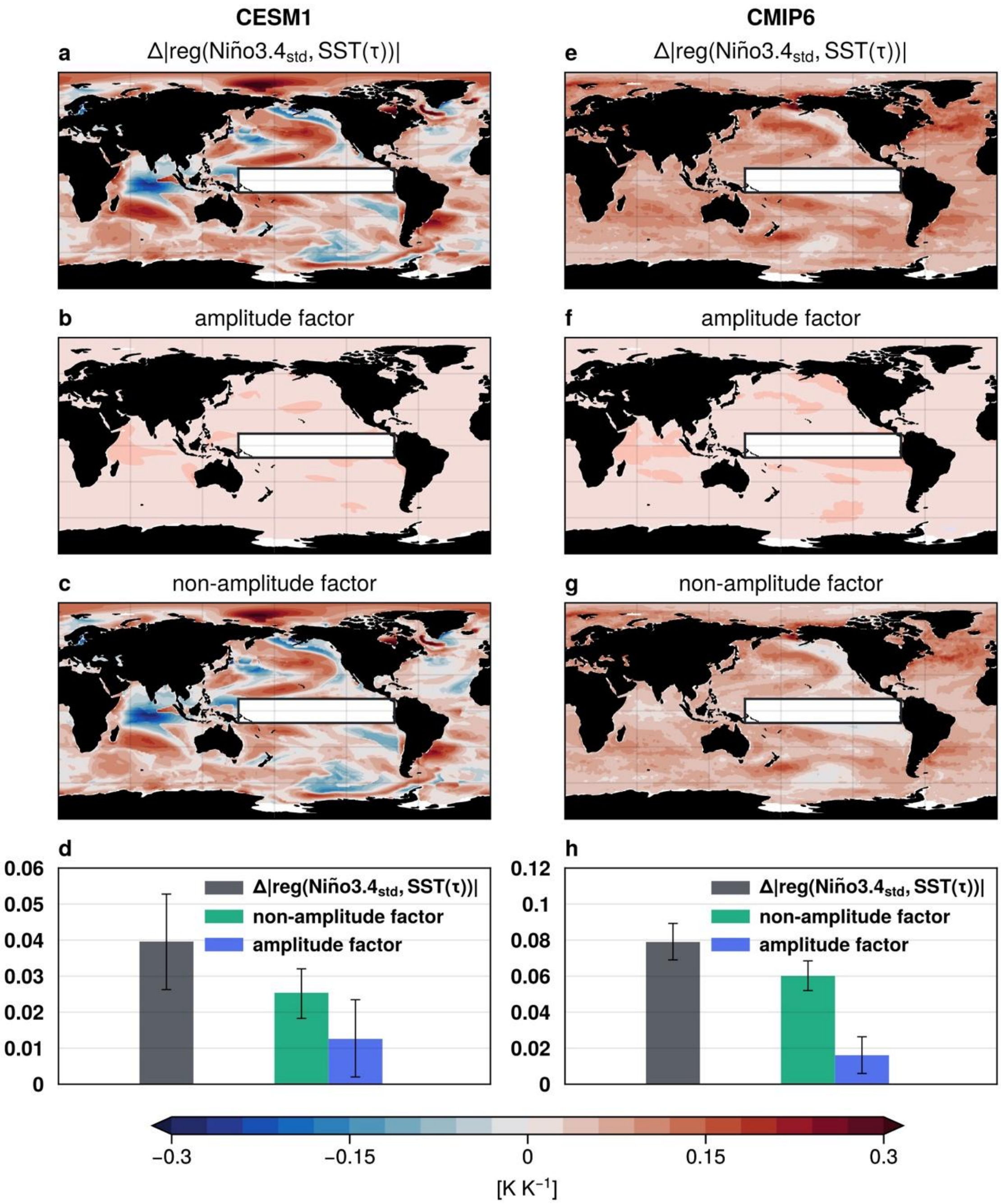

Fig. R1-1 | Decomposition of the changes in ENSO impacts on SST. a The changes in absolute values of SSTA(τ) regressed onto DJF Nino3.4 SSTA from the PD period to 2100. The contribution of **b** amplitude factor and **c** non-amplitude factor. **d** Global mean of (1) the changes in absolute values of SSTA(τ) regressed onto DJF Nino3.4 SSTA from the PD period to 2100, (2) non-amplitude factor, and (3) amplitude factor. **e-h** are the same as a-d (respectively) but CMIP6 multi-model mean.

2. The authors attribute the enhanced SST variability associated with ENSO primarily to the strengthening of surface flux anomalies, particularly latent heat flux (LHF). Based on qualitative analysis, they argue that the increase in global-mean LHF anomalies is driven by both enhanced climatological air-sea humidity differences and strengthened ENSO-induced surface wind anomalies. However, for several key regions, the analysis lacks sufficient quantitative support to convincingly identify the dominant physical drivers. Merely showing the spatial patterns of total LHF and wind anomalies is not adequate to substantiate the claim (Lines 201–203) that "the East CS, U.S. East Coast, and SNP are primarily attributed to anomalous wind variations, whereas the SIO is influenced by humidity changes." For instance, over the U.S. East Coast, the climatological specific humidity contrast (qs – qa) shows a substantial increase, which could potentially contribute more to the LHF anomalies than wind speed changes. Similarly, the changes in the SIO region may not be solely governed by the increase in anomalous humidity gradient. I therefore strongly recommend that the authors perform a more detailed quantitative analysis using the bulk formula for LHF to examine the contributions from changes in wind speed anomaly, climatological qs – qa, and ENSO-induced humidity gradient anomaly, and other relevant factors. The authors could refer to Lin et al. (2024) for relevant diagnostic approaches and analyses.

Ans) To address the reviewer's concern, we implemented a bulk–aerodynamic decomposition of the ENSO-related latent heat flux change from PD to 2100 and then translated latent heat flux to SST using our mixed-layer heat budget framework following Lin et al. (2024). And we added this kind of method to the Extended Data Text.

Decomposition of El Niño-induced latent heat flux anomalies

We decompose the changes in El Niño-induced latent heat flux ($\Delta Q'_{LH}$) following Lin et al. (2024), using the bulk formula equation:

$$\Delta Q'_{LH} \approx \Delta[-\rho_0 L C_e U(q_s - q_a)]'$$
$$= -\rho_0 L C_e \Delta[\overline{U}(q_s - q_a)'] - \rho_0 L C_e \Delta\left[U'\overline{(q_s - q_a)}\right] - \rho_0 L C_e \Delta[U'(q_s - q_a)'], \qquad (S4)$$

where Δ denotes the difference between PD and 2100 period. ρ_0 is air density (1 kg m^{-3}), L is latent heat vaporization (2.5 × 10^{6} J kg^{-1}), Ce is the turbulent exchange coefficient (1.4 × 10^{-3}), U is the 10 m wind speed, q_s is the saturation specific humidity at ocean surface, and q_a is 2 m air specific humidity. Since the third term (nonlinear term) of Eq. S4 is negligible, we further decompose the first, and second term as follows:

$$-\rho_0 L C_e \Delta[\overline{U}(q_s - q_a)'] \approx -\rho_0 L C_e \Delta\overline{U}(q_s - q_a)' - \rho_0 L C_e \overline{U}\Delta(q_s - q_a)' + R_1, \qquad (S5)$$

$$-\rho_0 L C_e \Delta\left[U'\overline{(q_s - q_a)}\right] \approx -\rho_0 L C_e \Delta U'\overline{(q_s - q_a)} - \rho_0 L C_e U'\Delta\overline{(q_s - q_a)} + R_2, \qquad (S6)$$

where an overbar and a prime (') denote climatology and the regression coefficient onto DJF Niño3.4, respectively. R_1 and R_2 are residuals, including each nonlinear term.

The decomposition is reported, in this order, into four contributions: (1) climatological wind speed, (2) El Niño–induced specific-humidity gradient, (3) El Niño–induced wind speed, and (4) climatological specific-humidity gradient, with a small residual for non-linear terms. Applied to the four key regions, Figure R1-2 shows time-integrated contributions of the decomposed terms from MAM(0) to τ (timing of maximum changes in R^2 values from MAM(0), see Main text methods for details). This reveals that the El Niño-induced wind speed contribution is the dominant amplifier outside the South Indian Ocean (SIO): it explains ~30% of the net change in the East China Sea (EastCS), ~72% along the U.S. East Coast, and ~119% in the Subtropical North Pacific (SNP; exceeding 100% because it offsets a damping of ENSO-induced humidity difference term).

In the SIO, by contrast, the leading contribution is the increase in the climatological specific-humidity gradient (~54%), consistent with enlarged climatological specific humidity gradient; the El Niño–driven humidity-gradient anomaly provides an additional ~33% (Extended Data Fig. 7). Two secondary patterns refine our interpretation: the El Niño–induced specific-humidity gradient provides an additional positive contribution in the EastCS (~65%), whereas it damps the response in the SNP (–38%). Although the ENSO-driven anomaly in the air–sea specific-humidity difference, $\Delta(q_s–q_a)'$, can be quantitatively important at regional scales, it cannot, by itself, account for the global amplification of ENSO-induced SST variability. Finally, the increase in the climatological air–sea humidity contrast contributes to ENSO-induced SSTA across all four regions and therefore qualitatively contributes to the amplification of ENSO-induced SST variability, even where its quantitative role is secondary (outside the SIO).

Taken together, these diagnostics corroborate our statement that strengthened winds are the prevailing driver of the amplified ENSO-SST variability in most regions, while background humidity increases are most important in the SIO. We have integrated these results into the revised Results section and Extended Data Text. Some elements here overlap with the following specific comments, the *Lines 186–203*, please cross-reference both sections. Here, δq indicates q_s–q_a.

(L189-208): While Figures 2 and 3 provide a global overview of sensitivity changes, a regional perspective reveals that El Niño–induced SST anomalies intensify under warming across four representative basins—the East China Sea (EastCS), the U.S. East Coast, the South Indian Ocean (SIO), and the subtropical North Pacific (SNP)—with the amplification primarily driven by ENSO-induced latent heat flux changes ($\Delta Q'_{LH}$) (Fig. 4; Extended Data Fig. 7). In the EastCS, an intensified western North Pacific anticyclone during D(0)JF(1)–MAM(1) weakens the climatological northwesterlies and reduces evaporation, yielding warmer SSTA (Fig. 4b; Extended Data Fig. 8 and 9). Along the U.S. East Coast, stronger ENSO-induced westerlies from ASO(0) to JFM(1) increase wind speed and enhance local evaporation, producing pronounced cooling that peaks in FMA(1) (Fig. 4c; Extended Data Fig. 8, and 9). In the SIO, by contrast, evaporation decreases and warmer SSTAs develop (Fig. 4d), primarily governed by increases in climatological δq rather than by ENSO-induced wind speed (Extended Data Fig. 9 and 11). The SNP experiences cooler SST (Fig. 4e), as strengthened ENSO-induced winds align with the trade winds from ND(0)J(1) to AMJ(1)**,** increasing wind speed and evaporation; here, ENSO-induced wind speed changes lead**,** whereas ENSO-induced δq acts as a damping (Extended Data Fig. 8-10). Across regions, MLD changes are secondary. Collectively, these results indicate that changes in the background δq—which modulate the efficacy of latent heat fluxes—together with stronger, region-dependent ENSO-induced wind anomalies, lead to an overall amplification of El Niño's SST impacts (see Extended Data Text for quantitative shares and seasonal phasing).

(Extended Data Text, L49-95):

Regional mechanisms behind the changes in ENSO-induced latent heat flux

To illuminate the physical pathways underlying the regional amplification of El Niño–induced SST anomalies, we examine four representative basins—the East China Sea (EastCS), the U.S. East Coast, the South Indian Ocean (SIO), and the subtropical North Pacific (SNP)—where impacts are evident in the PD simulation and intensify under warming (Fig. 4). Because we found that the changes in ENSO-induced SSTA of all the four regions are dominated by ENSO-induced latent heat flux ($\Delta Q'_{LH}$, Extended Data Fig. 7; EastCS ~65%, U.S. East Coast ~81%, SIO ~124%, and SNP ~59%), we further decompose the $\Delta Q'_{LH}$: the changes in climatological wind speed, climatological δq, ENSO-induced wind speed anomalies, and ENSO-induced δq, following the bulk-aerodynamic framework of Lin et al. (2024).

In the EastCS, during El Niño, particularly from D(0)JF(1) to MAM(1), an intensified anomalous western North Pacific anticyclone extends further northeastward and weakens climatological northwesterly (Extended Data Figs. 8a, i and 10). This weakening reinforces the increase in $\Delta Q'_{LH}$ (downward positive, i.e., reduced evaporation) via two pathways: (i) a larger negative wind speed anomaly, and (ii) a larger positive ENSO-induced q_a anomaly that reduces δq. Both effects suppress evaporation and thus promote stronger warm SSTA, peaking in MAM(1)[46] (Fig.4b and Extended Data Figs. 7 and 9). The U.S. East Coast is predominantly influenced by enhanced ENSO-induced wind speed (~72%) and climatological δq (~26%) variations (Extended Data Fig. 9b). From ASO(0) to JFM(1), stronger westerly winds enhance local evaporation (Extended Data Figs. 8b, f, 10b, j), resulting in significant cooling and a cold SSTA that peaks in FMA(1).

In the SIO, $\Delta Q'_{LH}$ accounts for 124% of the warm ΔSST_{SFC} because they are partially counterbalanced by reduced shortwave heating ($\Delta Q'_{SW} \approx$ -88%) associated with cloud[47], which is in turn largely offset by increased longwave heating ($\Delta Q'_{LW} \approx$ +60%). Within $\Delta Q'_{LH}$, humidity difference effects dominate (climatological ~54%; ENSO-induced ~33%), whereas the ENSO-induced wind speed term is net negative (~ -13%; Extended Data Fig.9c). The SIO shows climatological easterlies; during ENSO development, the resulting weak northeasterly anomalies (Extended Data Fig. 11) advect moister air into the region, suppressing evaporation, and reinforcing the warm SSTA while the wind speed anomalies remain weak negative. In the decay phase, ENSO-induced westerlies oppose the climatological easterlies and reduce wind speed, while warm SSTA raises ENSO-induced δq, which acts as a cooling contribution (Extended Data Fig. 8). Even so, the combined effect remains positive in both phases, and the changes in climatological δq always acts as a positive effect to increase in $\Delta Q'_{LH}$.

The SNP experiences cooler SSTA in future climate, driven by $\Delta Q'_{LH}$, especially the changes in ENSO-induced wind speed (~119%), while the changes in ENSO-induced δq act as a damping (~ -38%, Extended Data Fig. 9). Because the change in ENSO-induced wind from ND(0)J(1) to AMJ(1) not only becomes stronger but also aligns with the trade wind, significantly increasing wind speed in SNP (Extended Data Fig. 7, 8, and 9). In contrast, ENSO-induced δq damps the SST, because much cooler SSTA reduces q_s. Across regions, the changes in MLD have a relatively larger contribution in the SIO and SNP compared to the EastCS and U.S. East Coast, yet the contributions are insignificant across all regions. Overall, each region exhibits distinct seasonal characteristics and dominant contributing factors: the U.S. East Coast, and SNP are dominated by ENSO-induced wind changes, whereas the EastCS and SIO are shaped mainly by ENSO-induced and climatological δq, respectively. Although ENSO-induced δq can be sizable locally, only the climatological humidity difference consistently contributes positively across all four regions, indicating that the global-scale enhancement of ENSO-SST variability is not driven by ENSO-induced δq but by robust increases in the climatological δq.

Lin, S., Dong, B. & Yang, S. Enhanced Impacts of ENSO on the Southeast Asian Summer Monsoon Under Global Warming and Associated Mechanisms. Geophysical Research Letters 51, e2023GL106437 (2024).

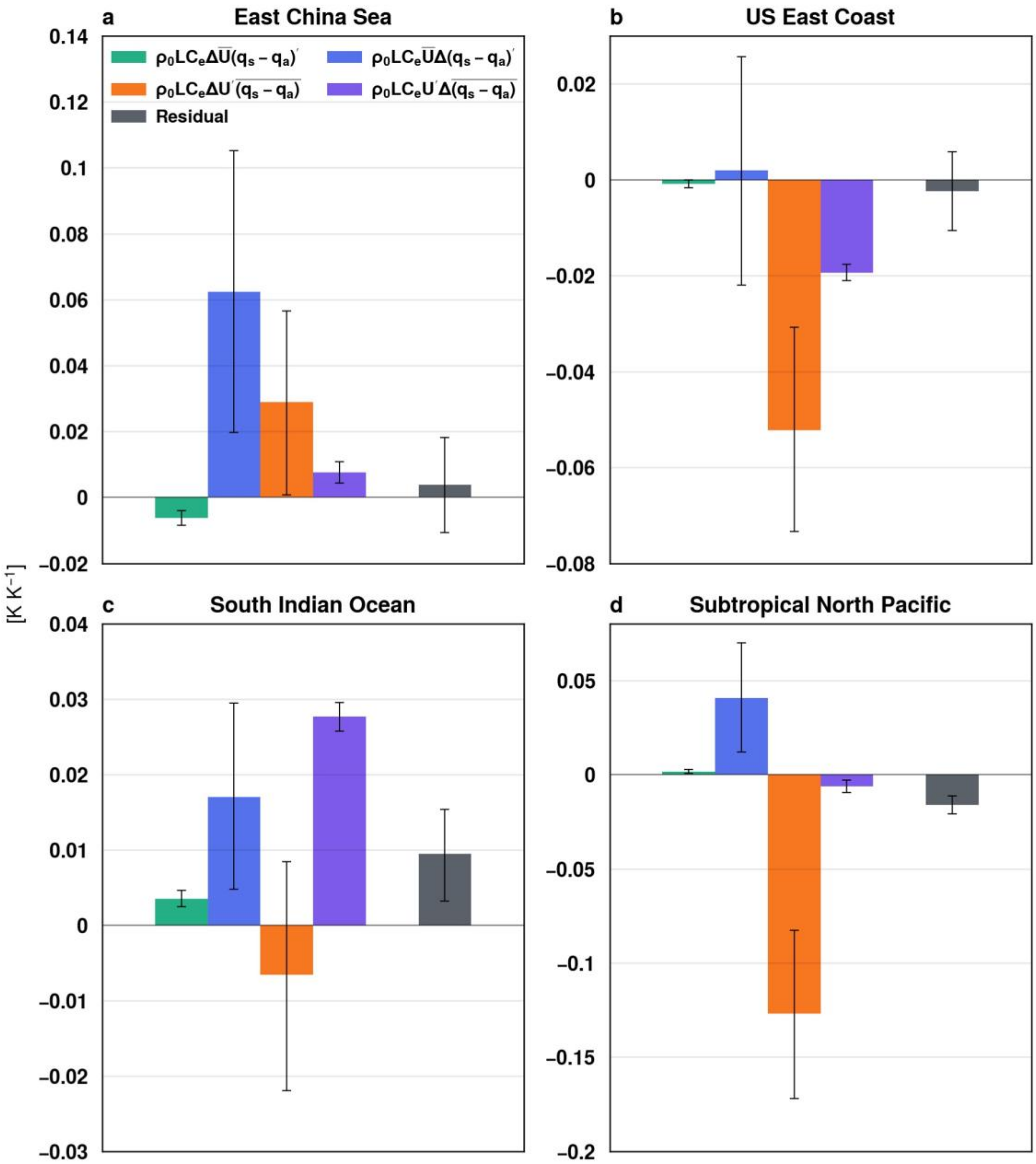

Fig. R1-2 | Decomposition of changes in ENSO-related latent heat flux contribution to SST in four key regions. Panels show four regions: **a** East China Sea (125°E–145°E, 20°N–35°N), **b** U.S. east coast (60°W–80°W, 25°N–40°N), **c** South Indian Ocean (50°E–90°E, 40°S–20°S), and **d** the subtropical North Pacific (150°E–165°W, 12°N–22°N). Bars quantify the PD to 2100 change in the contribution to ENSO-related latent heat flux-induced SST; climatological wind speed (green), El Niño–induced specific-humidity gradient (blue), El Niño–induced wind speed (yellow), and climatological specific-humidity gradient (purple); the gray bar is the residual. Error bars denote 95% confidence intervals from bootstrap test.

3. It is well known that El Niño and La Niña are asymmetric in terms of the center of SSTA, amplitude, persistence, and other characteristics, leading to their distinct and asymmetric impacts on the global climate. However, the current analysis is primarily based on correlation or regression methods, which implicitly assume linearity and overlook the influence of ENSO asymmetry. Therefore, I think that the authors should examine the composite changes in global SST separately for El Niño and La Niña events. At the very least, they should acknowledge this limitation and provide a brief discussion of its potential implications for their results.

Ans) To assess this explicitly, we constructed separate composites of global SST anomalies for El Niño and La Niña events for the PD and for 2100, and we further examined the change in their absolute values (|2100|–|PD|; Fig. R1-3). Events are defined by DJF Niño-3.4 SSTA exceeding ±1 standard deviation (≥+1σ for El Niño; ≤−1σ for La Niña), and the temporal alignment follows the same protocol as the maximum R^2 analysis (Methods). Here, however, we analyze composite amplitudes rather than correlations.

The composites reproduce the canonical asymmetries between El Niño and La Niña in teleconnections and show that the projected changes are themselves asymmetric. For El Niño, the SST response strengthens over most ocean basins, broadly consistent with our linear regression results. For La Niña, although the global-mean amplitude also increases, the local pattern of change differs: the influence weakens over the Kuroshio–Oyashio Extension east of Japan, while it strengthens in several regions—including the North Pacific, the South Pacific Convergence Zone, and the Maritime Continent—in some cases exceeding the corresponding El Niño enhancement. We acknowledge this El Niño–La Niña teleconnection asymmetry and have revised the Discussion section to explicitly note this point.

(L230-234): Additionally, to address the ENSO asymmetry, we further examined El Niño and La Niña composites separately; in both cases, the SST response increases under warming, yet the regional patterns are asymmetric. Although a more detailed analysis is needed to fully interpret the asymmetries, it is clear that the SST impacts in both El Nino and La Nina cases increase.

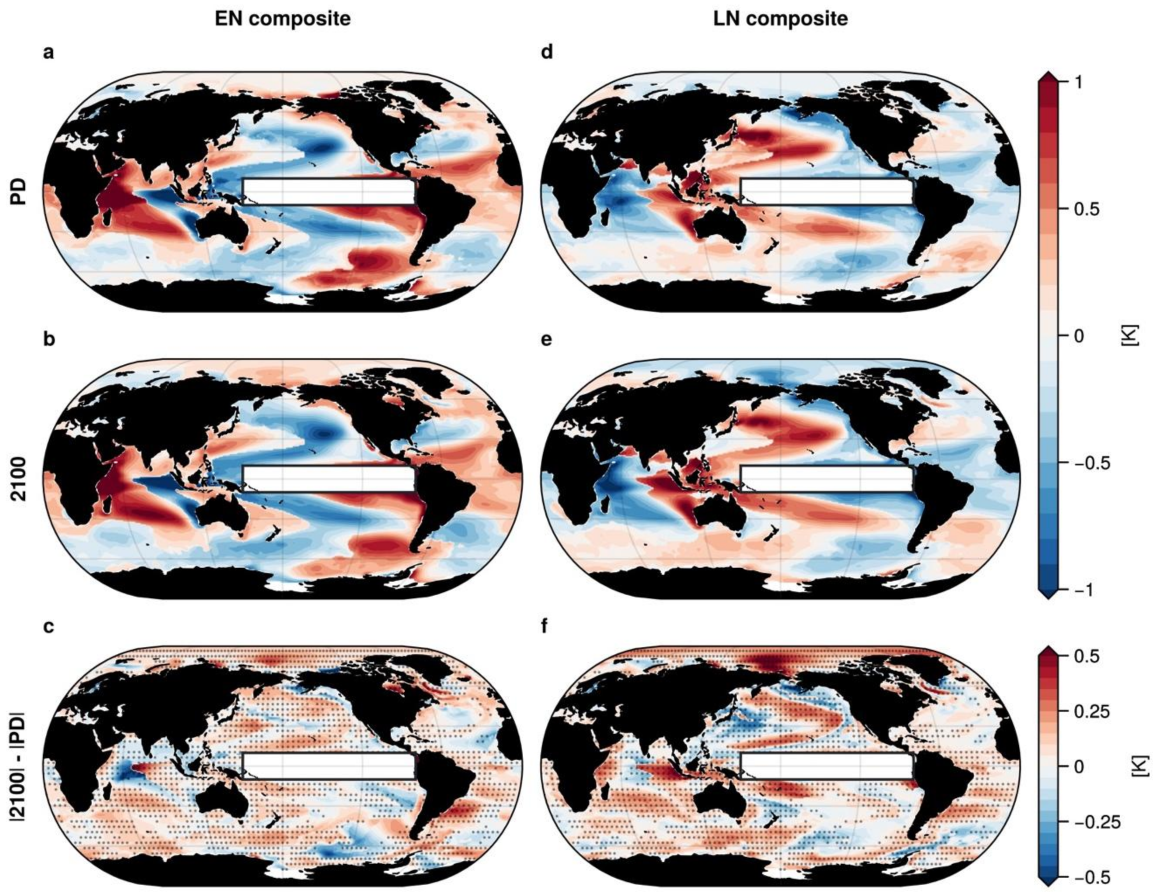

Fig. R1-3 | Changes in El Niño and La Niña impacts on SST. a-c El Niño composites for PD, 2100, and the change in absolute magnitude (|2100|-|PD|), taking the absolute maximum over the JJA(0)–JJA(1). **d-f** As in a-c but for La Niña. Stippling denotes regions where the change in absolute amplitude is statistically significant at the 95% confidence level using a bootstrap test. The white box marks the equatorial Pacific region to exclude ENSO SST itself.

4. I noticed that the equatorial Indian Ocean exhibits a significant decrease in ENSO-induced SST variability. However, both surface wind speed and the climatological humidity gradient in this region are projected to strengthen under global warming, which suggests that changes in LHF anomalies alone may not fully explain the reduced SST variability there. Do the authors have a plausible explanation for this contrasting behavior? What mechanisms might be responsible for the weakened ENSO-induced SST variability in this region, especially given the overall strengthening of ENSO impacts observed elsewhere?

Ans) Thanks for asking an important question. Figure R1-4 examines the equatorial Indian Ocean and contrasts four diagnostics—SST_{TOT}, $SST_{SFC+MLD}$, SST_{SFC}, and SST_{MLD}—together with time series of SST regressed onto the DJF Niño3.4 SSTA. The gap between SST_{TOT} and $SST_{SFC+MLD}$ indicates a substantial contribution from ocean dynamics in this region. Consistent with previous studies, El Niño is linked to Indian Ocean variability through two phases: during the growth phase, as well as the atmospheric heat flux, dynamical processes (thermocline shoaling/upwelling and associated circulation changes) promote a positive Bjerknes feedback (Bjerknes, 1969) fosters development of the Indian Ocean Dipole (IOD) and enhance cooling in the eastern equatorial basin (Saji et al., 1999); during the decay phase, surface heat-flux anomalies favor the Indian Ocean Basin Mode (IOBM) and yield basin-wide warming (Cai et al, 2019 and Klein et al, 1999).

Because our primary decomposition isolates the surface flux pathway, the growing-phase dynamical cooling is not fully captured, implying that our thermodynamic estimate is not adequate to fully explain SST evolution. This interpretation is supported by the diagnostics: SST_{TOT} shows stronger cooling than $SST_{SFC+MLD}$, consistent with an enhanced dynamical contribution, whereas SST_{SFC} indicates that the surface flux pathway itself strengthens under warming. Taken together, these results suggest that the overall El Niño influence on the equatorial Indian Ocean intensifies, but the decaying-phase warm SST anomaly becomes weaker in 2100. This attenuation explains why the signal over the equatorial Indian Ocean appears muted (and locally cooler) despite the increased ENSO impact.

The time series shows El Niño’s stronger impacts on Indian Ocean cooling in SON(0) and weaker impacts on Indian Ocean warming in D(0)JF(1) to JJA(1).

Bjerknes, J. ATMOSPHERIC TELECONNECTIONS FROM THE EQUATORIAL PACIFIC. *Monthly Weather Review* **97**, 163–172 (1969).

Cai, W. *et al.* Pantropical climate interactions. *Science* **363**, eaav4236 (2019).

Saji, N. H., Goswami, B. N., Vinayachandran, P. N. & Yamagata, T. A dipole mode in the tropical Indian Ocean. *Nature* **401**, 360–363 (1999).

Klein, S. A., Soden, B. J. & Lau, N.-C. Remote Sea Surface Temperature Variations during ENSO: Evidence for a Tropical Atmospheric Bridge. (1999).

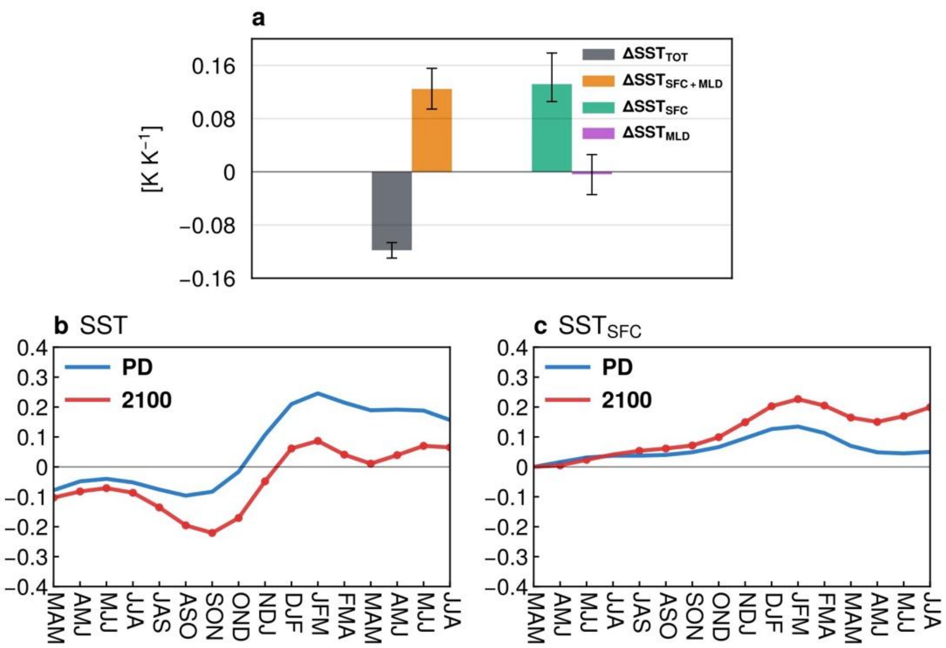

Fig. R1-4 | The mechanisms of decrease in El Niño impact on Indian Ocean SST variability. a Same as Extended Fig. 5a for Equatorial Indian Ocean (60°E–85°E, 10°S–5°N). **b** Temporal evolution of SSTA regressed onto DJF Niño3.4 SSTA from MAM(0) to JJA(1), during PD (blue line) and the 2100 period (red line) for the equatorial Indian Ocean. **c** Temporal evolution of SSTA changed by the only El Niño-induced surface flux (conducted with SFC regressed on DJF Niño3.4 SSTA). Red dots indicate statistically significant at the 95% confidence level using the bootstrap test.

Specific comments:

Lines 40–42: Consider citing some references here to support the statement, such as recent studies on the enhanced impact of ENSO on East Asian climate under global warming (e.g., Lin et al. 2024).

Ans) We have added recent studies such as Lin et al. 2024, and Cai et al. 2020.

Lin, S., Dong, B. & Yang, S. Enhanced Impacts of ENSO on the Southeast Asian Summer Monsoon Under Global Warming and Associated Mechanisms. Geophysical Research Letters 51, e2023GL106437 (2024).

Cai, W. et al. Climate impacts of the El Niño–Southern Oscillation on South America. Nat Rev Earth Environ 1, 215–231 (2020).

Lines 57–59: I also suggest citing more recent literature to support this point.

Ans) We have added recent studies (Power et al. 2013, Yun et al. 2021, Zhou et al. 2014, and Hu et al. 2021).

Power, S., Delage, F., Chung, C., Kociuba, G. & Keay, K. Robust twenty-first-century projections of El Niño and related precipitation variability. *Nature* **502**, 541–545 (2013).

Yun, K.-S. et al. Increasing ENSO–rainfall variability due to changes in future tropical temperature–rainfall relationship. *Commun Earth Environ* **2**, 1–7 (2021).

Zhou, Z.-Q., Xie, S.-P., Zheng, X.-T., Liu, Q. & Wang, H. Global Warming–Induced Changes in El Niño Teleconnections over the North Pacific and North America. *Journal of Climate* **27**, 9050–9064 (2014).

Hu, K., Huang, G., Huang, P., Kosaka, Y. & Xie, S.-P. Intensification of El Niño-induced atmospheric anomalies under greenhouse warming. *Nat. Geosci.* **14**, 377–382 (2021).

Line 72: It is unclear whether this refers to a 3-month mean SSTA or a 3-month running mean SSTA. This should be clarified, as the method section (Line 281) seems to indicate the latter.

Ans) Revised the manuscript to "3-month running mean SSTA"

Lines 133–138 & Extended Data Fig. 4: It is difficult to conclude from this figure that the increased SFC are dominated by longwave radiation induced by ENSO. Please add the difference between the 2100 and PD to help support this claim.

Ans) Thank you for the helpful suggestion. We now explicitly quantify the PD to 2100 difference. Figure R1-5e shows the global mean of the shortwave and longwave radiative contributions to the SST_{SFC} (Fig. R1-5 and Extended Data Fig. 5).

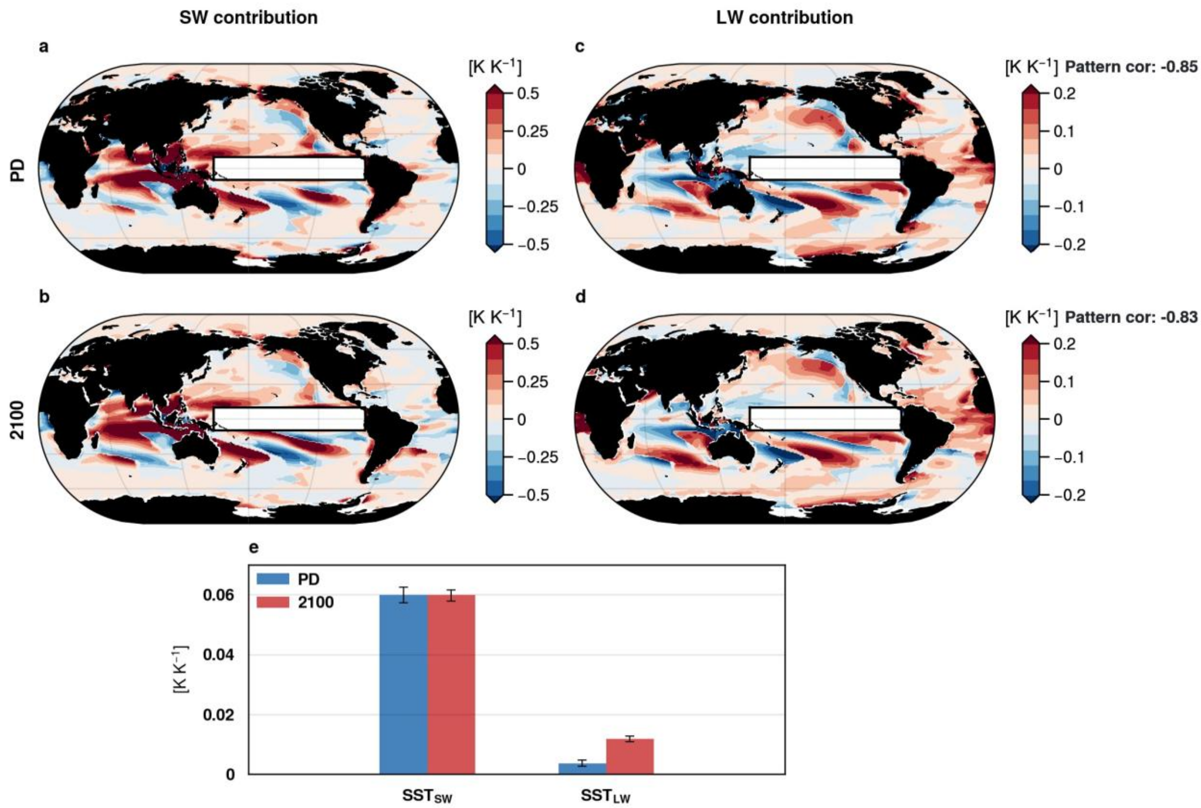

Fig. R1-5 | Compensation between the contributions of El Niño-induced shortwave and longwave radiation to global SST. a Shortwave radiation contribution to SSTSFC+MLD during PD period in CESM1. **b** Same as a but during 2100. **c-d** Same as a and b, but longwave radiation. **e** Global mean of shortwave radiation contribution (left) and longwave radiation contribution (right) in PD and 2100 period. Error bars are calculated at the 95% confidence level using a bootstrap test.

Line 144: Consider changing "moisture anomalies" to "mean moisture," if referring to the background state.

Ans) Revised to "mean moisture"

Lines 165–166: Do you mean the mean or the anomaly of the specific humidity difference (qs – qa)? I believe the intended meaning may be the change in the climatological humidity gradient. Please clarify.

Ans) Revised to "mean specific humidity difference"

Extended Data Fig. 5: The labels are too small, making the figure difficult to read. The authors may want to adjust the panel layout to enlarge each subplot and improve legibility.

Ans) We adjusted the panel layout of Extended Data Fig. 5 (Now, Extended Data Fig. 7; Fig. R1-6).

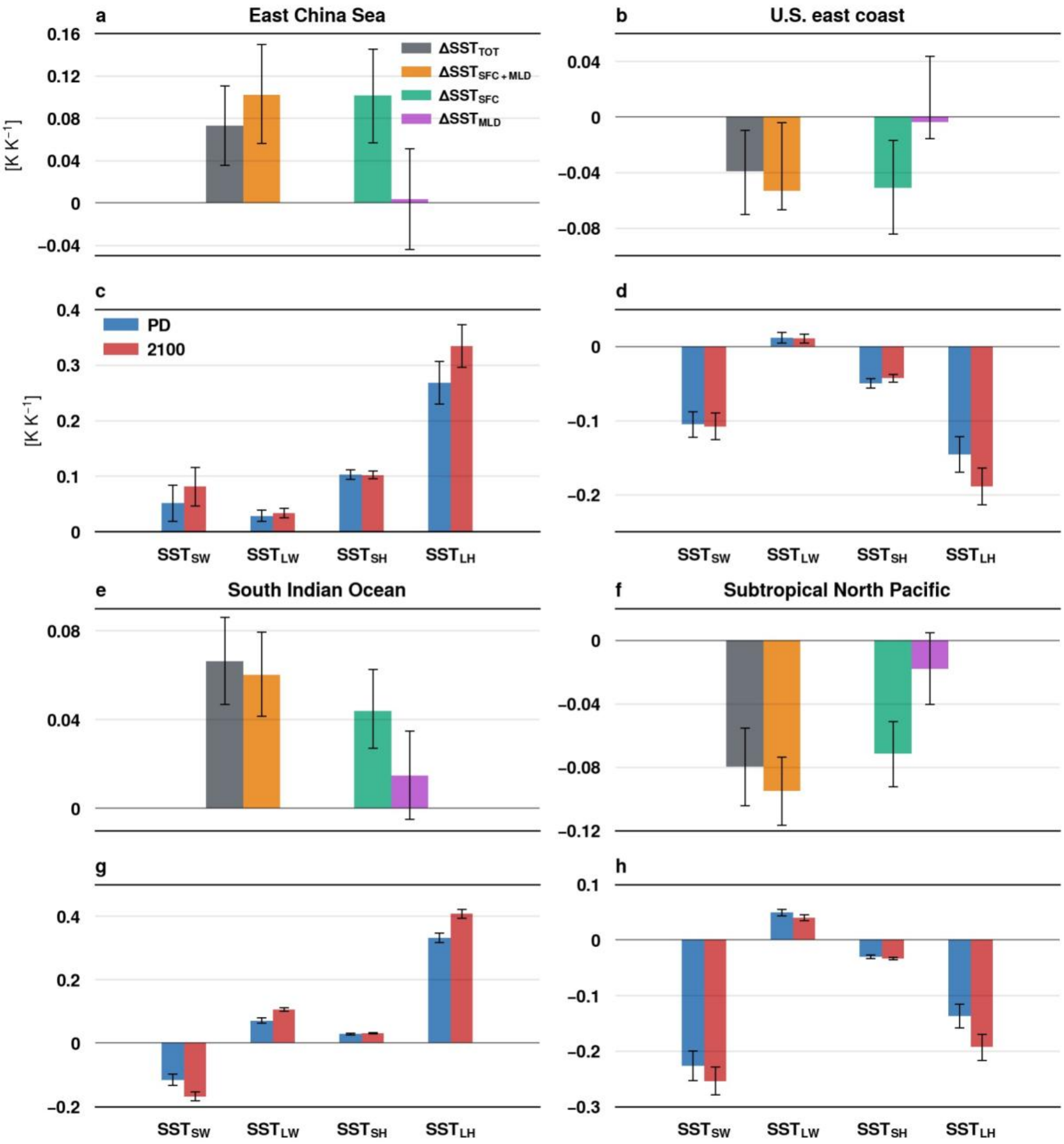

Fig. R1-6 | The changes in contributors of the global El Niño impacts on SST at each region. a, b, e and **f** Same as Fig. 2b but the integrated term before multiplied by the sign of SST_{TOT} ($\Delta SST_{SFC+MLD}$, ΔSST_{SFC}, and ΔSST_{MLD}) and ΔSST_{TOT} is not absolute value (see Methods for details) for each region: **a** East China Sea (125°E–145°E, 20°N–35°N), **b** U.S. east coast (60°W–80°W, 25°N–40°N), **e** South Indian Ocean (50°E–90°E, 40°S–20°S), and **f** the subtropical North Pacific (150°E–165°W, 12°N–22°N). **c**, **d**, **g,** and **h** The same as Fig. 2c, but for each region: **c** East China Sea, **d** U.S. east coast, **g** South Indian Ocean, and **h** the subtropical North Pacific rather than global mean.

Lines 186–203: The change in latent heat flux anomalies can result from variations in wind speed, climatological humidity gradient, or the anomalous humidity gradient. In particular, over the U.S. East Coast, the increase in the climatological humidity gradient is substantial, yet no quantitative evidence is provided, and only the conclusion that wind anomalies dominate is stated. I recommend that the authors conduct a quantitative decomposition using the bulk formula for LHF to support their interpretation. In addition, including a time series plot (similar to Fig. 4) that illustrates the evolution of LHF anomalies and their components (e.g., wind speed, qs – qa) during the development and decay phases of ENSO would help elucidate the physical processes for the reader.

Ans) Following the reviewer's suggestion, we quantitatively decomposed the change in ENSO-related latent heat flux anomalies from PD to 2100 using the bulk aerodynamic formula and examined the seasonal evolution of each term (Fig. R1-7). Across all four regions, the contribution from ENSO-induced wind-speed anomalies is substantial and generally dominant. In the East China Sea, the ENSO-driven humidity-gradient anomaly makes an additional sizeable contribution during D(0)JF(1)–MAM(0). Along the U.S. East Coast, the results most closely follow our main mechanism: the strengthened El Niño wind-speed anomaly is the leading amplifier, while the increased climatological air–sea humidity contrast provides a secondary positive effect. In the South Indian Ocean, the humidity-gradient anomaly contributes to warming during the development phase, whereas from D(0)JF(1) the decrease in wind speed becomes the main positive (warming) contributor; over the same period the ENSO-driven humidity-gradient anomaly acts as a damping term, while the climatological humidity gradient contributes positively throughout. In the Subtropical North Pacific, enhanced El Niño wind-speed anomalies again dominate, and the ENSO-driven humidity-gradient anomaly damps the response, consistent with larger SST-driven humidity changes there.

(L189-208): While Figures 2 and 3 provide a global overview of sensitivity changes, a regional perspective reveals that El Niño–induced SST anomalies intensify under warming across four representative basins—the East China Sea (EastCS), the U.S. East Coast, the South Indian Ocean (SIO), and the subtropical North Pacific (SNP)—with the amplification primarily driven by ENSO-induced latent heat flux changes ($\Delta Q'_{LH}$) (Fig. 4; Extended Data Fig. 7). In the EastCS, an intensified western North Pacific anticyclone during D(0)JF(1)–MAM(1) weakens the climatological northwesterlies and reduces evaporation, yielding warmer SSTA (Fig. 4b;

Extended Data Fig. 8 and 9). Along the U.S. East Coast, stronger ENSO-induced westerlies from ASO(0) to JFM(1) increase wind speed and enhance local evaporation, producing pronounced cooling that peaks in FMA(1) (Fig. 4c; Extended Data Fig. 8, and 9). In the SIO, by contrast, evaporation decreases and warmer SSTAs develop (Fig. 4d), primarily governed by increases in climatological δq rather than by ENSO-induced wind speed (Extended Data Fig. 9 and 11). The SNP experiences cooler SST (Fig. 4e), as strengthened ENSO-induced winds align with the trade winds from ND(0)J(1) to AMJ(1)**,** increasing wind speed and evaporation; here, ENSO-induced wind speed changes lead**,** whereas ENSO-induced δq acts as a damping (Extended Data Fig. 8-10). Across regions, MLD changes are secondary. Collectively, these results indicate that changes in the background δq—which modulate the efficacy of latent heat fluxes—together with stronger, region-dependent ENSO-induced wind anomalies, lead to an overall amplification of El Niño's SST impacts (see Extended Data Text for quantitative shares and seasonal phasing).

(Extended Data Text, L49-95):

Regional mechanisms behind the changes in ENSO-induced latent heat flux

To illuminate the physical pathways underlying the regional amplification of El Niño–induced SST anomalies, we examine four representative basins—the East China Sea (EastCS), the U.S. East Coast, the South Indian Ocean (SIO), and the subtropical North Pacific (SNP)—where impacts are evident in the PD simulation and intensify under warming (Fig. 4). Because we found that the changes in ENSO-induced SSTA of all the four regions are dominated by ENSO-induced latent heat flux ($\Delta Q'_{LH}$, Extended Data Fig. 7; EastCS ~65%, U.S. East Coast ~81%, SIO ~124%, and SNP ~59%), we further decompose the $\Delta Q'_{LH}$: the changes in climatological wind speed, climatological δq, ENSO-induced wind speed anomalies, and ENSO-induced δq, following the bulk-aerodynamic framework of Lin et al. (2024).

In the EastCS, during El Niño, particularly from D(0)JF(1) to MAM(1), an intensified anomalous western North Pacific anticyclone extends further northeastward and weakens climatological northwesterly (Extended Data Figs. 8a, i and 10). This weakening reinforces the increase in $\Delta Q'_{LH}$ (downward positive, i.e., reduced evaporation) via two pathways: (i) a larger negative wind speed anomaly, and (ii) a larger positive ENSO-induced q_a anomaly that reduces δq. Both effects suppress evaporation and thus promote stronger warm SSTA, peaking in

MAM(1)[46] (Fig.4b and Extended Data Figs. 7 and 9). The U.S. East Coast is predominantly influenced by enhanced ENSO-induced wind speed (~72%) and climatological δq (~26%) variations (Extended Data Fig. 9b). From ASO(0) to JFM(1), stronger westerly winds enhance local evaporation (Extended Data Figs. 8b, f, 10b, j), resulting in significant cooling and a cold SSTA that peaks in FMA(1).

In the SIO, $\Delta Q'_{LH}$ account for 124% of the warm ΔSST_{SFC} because they are partially counterbalanced by reduced shortwave heating ($\Delta Q'_{SW} \approx$ -88%) associated with cloud[47], which is in turn largely offset by increased longwave heating ($\Delta Q'_{LW} \approx$ +60%). Within $\Delta Q'_{LH}$, humidity difference effects dominate (climatological ~54%; ENSO-induced ~33%), whereas the ENSO-induced wind speed term is net negative (~ -13%; Extended Data Fig.9c). The SIO shows climatological easterlies; during ENSO development, the resulting weak northeasterly anomalies (Extended Data Fig. 11) advect moister air into the region, suppressing evaporation, and reinforcing the warm SSTA while the wind speed anomalies remain weak negative. In the decay phase, ENSO-induced westerlies oppose the climatological easterlies and reduce wind speed, while warm SSTA raises ENSO-induced δq, which acts as a cooling contribution (Extended Data Fig. 8). Even so, the combined effect remains positive in both phases, and the changes in climatological δq always acts as a positive effect to increase in $\Delta Q'_{LH}$.

The SNP experiences cooler SSTA in future climate, driven by $\Delta Q'_{LH}$, especially the changes in ENSO-induced wind speed (~119%), while the changes in ENSO-induced δq acts as a damping (~ -38%, Extended Data Fig. 9). Because the change in ENSO-induced wind from ND(0)J(1) to AMJ(1) not only becomes stronger but aligns with the trade wind, significantly increasing wind speed in SNP (Extended Data Fig. 7, 8 and 9). In contrast, ENSO-induced δq damps the SST, because much cooler SSTA reduces q_s. Across regions, the changes in MLD have a relatively larger contribution in the SIO and SNP compared to the EastCS and U.S. East Coast, yet the contributions are insignificant across all regions. Overall, each region exhibits distinct seasonal characteristics and dominant contributing factors: the U.S. East Coast, and SNP are dominated by ENSO-induced wind changes, whereas the EastCS and SIO are shaped mainly by ENSO-induced and climatological δq, respectively. Although ENSO-induced δq can be sizable locally, only the climatological humidity difference contributes consistently positively across all four regions, indicating that the global-scale enhancement of ENSO-SST variability is not driven by ENSO-induced δq but by robust increases in the climatological δq.

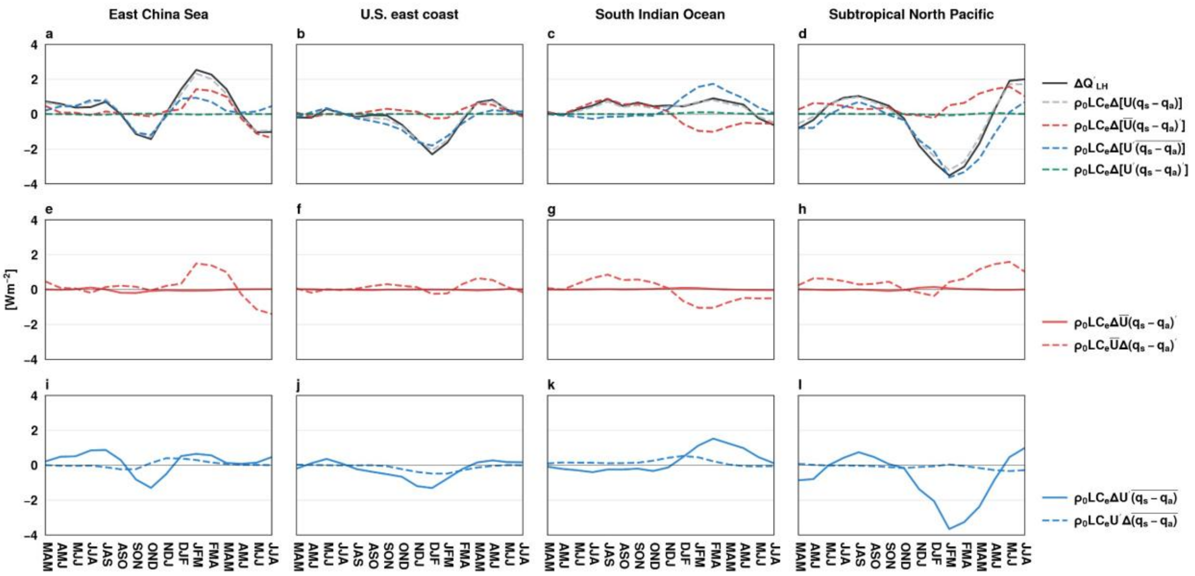

Fig. R1-7 | Time series of the changes in ENSO-induced latent heat flux. Seasonal evolution of the change in ENSO-related latent heat flux anomalies from PD to 2100 and its components for four regions: **a-d** East China Sea, U.S. East Coast, South Indian Ocean, and Subtropical North Pacific. The top row shows the total latent heat flux change (black) together with the reconstructed sum of components (gray dashed line). Red, blue, and green dashed line are each term of Eq. S4 (Extended Data for details). **e-h** The middle row separates the two terms that contain the ENSO-driven humidity-gradient anomaly (solid line), and the change in the climatological wind speed (dashed line). **i-l** The bottom row separates the two terms that contain the ENSO-induced wind-speed (solid curve) and the change in the climatological humidity difference (dashed line).

Line 291: How do the authors calculate the SST tendency? Is it estimated based on the mixed-layer heat budget equation, or directly quantified using the time tendency of mixed-layer SST from model output? Please clarify this in the manuscript.

Ans) We did not diagnose the model's full mixed-layer temperature tendency $\partial T_m/\partial t$ nor close the complete budget. Instead, we used the mixed-layer heat budget as a diagnostic framework and quantified only the surface flux-driven component of the ENSO-related SSTA by time-integrating the surface flux term:

$$SST_{SFC+MLD} = sign(SST_{TOT}) \times \int_{MAM(0)}^{\tau} \frac{Q'_{net}}{\rho_0 C_p \bar{h}} dt$$

$$SST_{SFC} = sign(SST_{TOT}) \times \int_{MAM(0)}^{\tau} \frac{Q'_{net}}{\rho_0 C_p \bar{h}_{PD}} dt$$

$$SST_{MLD} = sign(SST_{TOT}) \times \int_{MAM(0)}^{\tau} \frac{Q'_{net,PD}}{\rho_0 C_p \bar{h}} dt$$

Here, Q'_{net} is the regression coefficient of net surface flux with respect to DJF Niño3.4 SSTA, $\bar{h}$ is the climatological mixed layer depth to calculate $SST_{SFC+MLD}$. We further isolate effects as SST_{SFC} and SST_{MLD} so that changes in $\bar{h}$ and in Q'_{net} are separated. The residual (SST_{TOT} - $SST_{SFC+MLD}$) collects all non-surface flux processes such as horizontal/vertical advection, entrainment process, and diffusion. We have revised the Methods to explicitly state this and replaced phrases suggesting "SST tendency" with wording "surface flux-induced SSTA". We have also clarified this point in the revised manuscript.

(L306-313): We calculated the surface flux-induced SSTA in diagnostic framework, based on the following mixed layer heat budget equation:

$$\frac{\partial T_m}{\partial t} = \frac{Q_{net}}{\rho_0 C_p h} + Res, \quad (1)$$

where T_m is the mixed layer temperature, Q_{net} is net surface flux (positive into the ocean), ρ_0 (1027 kg m^{-3}) is the reference density of seawater, C_p (3985 J kg^{-1} K^{-1}) is the specific heat of seawater at constant pressure. We only used surface flux term and calculate the surface flux contribution to ENSO-driven SSTA. The Res mainly represents contributions from ocean dynamical processes such as horizontal/vertical advection, entrainment, and diffusion.

Line 300 & Figure 2: I am confused about the relationship between SSTSFC+MLD and SSTTOT. The integration of SFC from MAM to τ should correspond to the SST anomaly change from spring to τ, i.e., the difference between SSTTOT and SSTMAM. Therefore, in terms of magnitude, this difference may better correspond to the SSTSFC+MLD than SSTTOT alone.

Ans) Thank you for highlighting this inconsistency. In our framework, the surface-flux contribution ($SST_{SFC+MLD}$) is obtained by integrating from MAM(0) to τ and should therefore be compared with the change in SST over the same interval. While Figure 4 followed this convention, we inadvertently compared $SST_{SFC+MLD}$ with $SST_{TOT}(\tau)$ itself in Figure 2 and Extended Data Figures 2, 5, and 10. We have corrected all four figures to use the MAM(0) to τ change, which reduces the residual and improves model consistency. In response to the reviewer's comment, we have revised the Methods section as follows:

(L318-319): SST_{TOT} is the difference between the regression coefficient of SSTA with respect to DJF Niño3.4 SSTA at time τ and MAM(0)

Response to Reviewers #2 & #3

Reviewers #2

I co-reviewed this manuscript with one of the reviewers who provided the listed reports. This is part of the Nature Communications initiative to facilitate training in peer review and to provide appropriate recognition for Early Career Researchers who co-review manuscripts.

Reviewers #3

It is very interesting to see the novel analysis to find the maximum variance of the SST response (maximum R2 value), taking into account the time lag "tau", and the distribution of the wind speed response at the time when the ENSO effect is maximized. The finding is also new that the amplitude of influence of ENSO on SSTs increases globally with global warming. On the other hand, the interpretation of the mechanism seems to me to leave some questions unanswered, and I feel that the understanding of the process is not fully developed. The details are described below, but given the number of questionable aspects of the process and the possibility that the way the logic is constructed may need to be fundamentally revised, I would recommend that the paper be rejected and resubmitted after sufficient time for revision.

We would like to thank the reviewers for their careful and constructive suggestions, which helped to improve the quality of this manuscript. Our responses to the specific comments are as follows:

Comments:

1. The biggest question is that the pattern of wind speed response considering the lag "tau" remains the same whether it is EP or CP, and whether the ENSO amplitude is larger or smaller due to global warming (L220-L231, Fig. 3 and Extended Data Fig. 9). The only possible explanation for the agreement in those figures, even though the teleconnection patterns should clearly be different, is that the lag "tau" is different at each location. (Please show the spatial map of lag "tau" for EP and CP.) It seems to me that the process is no longer about the physics of the ENSO response, but we are simply seeing that the wind speed responses to any forcing *from the tropics appears to deviate with large anomalies at the same location at the same timing "tau" that matches the location where the amplitude of the climatological wind speed variation is large. Please plot the spatial map of the annual maxima of wind speed variance on a global map and see if they are consistent with Fig. 3 and Extended Data Fig. 9.*

Ans) Thank you for the important questions. As the reviewer noted, El Niño teleconnections can vary depending on ENSO pattern diversity, amplitude, phase (El Niño versus La Niña), and many other factors. The intention of our study is to highlight changes in ENSO impacts in an averaged sense across whole events. The observational global SST anomalies shown in Extended Data Fig. 1 exhibit the well-known pattern that has been consistently explained in previous literature, even though various ENSO types are mixed. Our model reproduces this observed pattern well, suggesting that our approach captures the underlying physical processes.

As the reviewer suggested, we now provide spatial maps of the lag τ that maximizes the 10 m wind speed regression onto Niño3.4, Niño3 (EP), and Niño4 (CP) SSTAs (Fig. R2-1a-c). The phase of the wind speed response is largely insensitive to the ENSO index used: EP and CP maps closely resemble the Niño3.4 result, and many regions (stippling) share the same τ.

Comparison with the calendar month of the 10 m wind speed variance maximum shows coincidence over only ~20% of the ocean area (Fig. R2-1d). Therefore, the ENSO-related wind speed patterns do not simply mirror where the climatological wind variance happens to peak. It reflects the seasonally phased teleconnection.

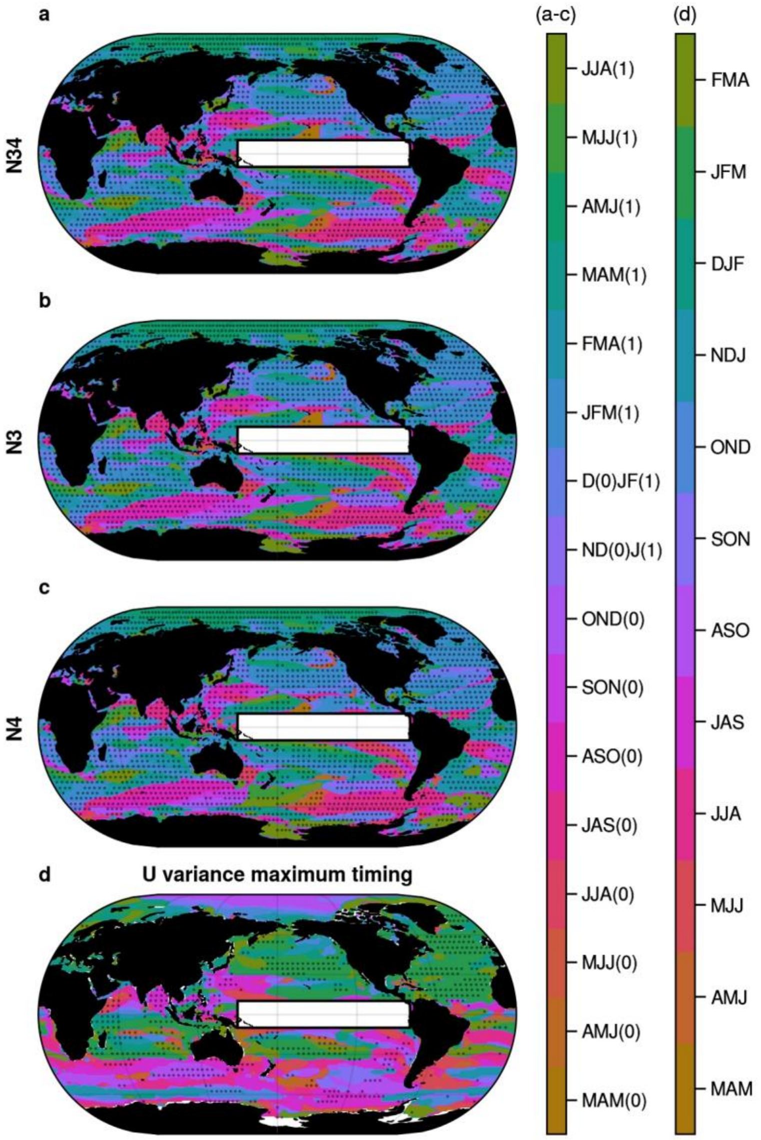

Fig. R2-1 | Phase of ENSO-related wind-speed response versus the climatological variance maximum. a-c, Calendar month of the maximum regression of 10 m wind speed onto Niño3.4, Niño3, and Niño4 SSTA. Stippling marks grid points where all three indices yield the same peak month. **d** Calendar month of the standard deviation, maximum of 3-month running mean 10 m wind speed; stippling indicates grid points where this month coincides with the ENSO peak month.

2. Regarding the similarity of the spatial pattern of the maximum R2 values in EP and in CP, it appears that the locations where the maximum R2 values are larger (Fig. 1 and Extended Data Fig. 8) correspond to locations where the climatological MLD is shallower (Extended Data Figure 3-a and b). It appears to me that this just means that the shallower the MLD is, the more sensitive it is to atmospheric Q_LH variation. Since the text only discusses the impact of MLD changes due to global warming, I believe that a logical connection is missing.

Ans) We thank the reviewer for this suggestion. The pattern correlation between the Present-day (PD) climatological mixed layer depth (MLD) and the peak R^2 is r = -0.05; the pattern correlation between PD climatological MLD and the change in peak R^2 is r = 0.02. Both values are nearly zero, indicating that regions of large peak R^2 and regions where peak R^2 increases are not systematically co-located with shallow MLD.

We agree with the physical intuition that, all else equal, a shallower mixed layer can heighten local SST sensitivity to surface fluxes. However, in our results the spatial structure of where ENSO explains the most variance—and where that influence strengthens—does not track PD MLD. This implies that MLD is at most a secondary modulator, and that other factors tied to ENSO forcing and air-sea coupling organize the pattern more strongly.

3. The same is true for changes due to global warming: is it possible that the amplitude of the general atmospheric teleconnection to any forcing from the tropics is increasing, and the "increased amplitude of response associated with ENSO" referred to in this paper is only a part of what we are seeing? If the above considerations (1) through (3) are true, then the logic construct and story structure of this paper, including the title, needs to be fundamentally revised. This will take time, which is why I have recommended a rejection and resubmission.

Ans) We sincerely appreciate the reviewer's insightful point that atmospheric teleconnections from the tropics to the globe may in general strengthen under global warming. We fully agree that such an amplification is plausible, given processes such as stronger wind responses arising from enhanced precipitation sensitivity to tropical SST anomalies and increased mean humidity differences in a warmer climate. These processes are not unique to ENSO and may indeed apply, to some extent, to other tropical variability modes.

Our study, however, focuses on ENSO for two main reasons. First, both observations and climate models consistently indicate that ENSO remains the most dominant, spatially extensive, and recurrent driver of interannual tropical–global SST variability. Second, while other modes such as Indian Ocean variability or Atlantic variability also produce teleconnections, their signals are generally smaller in amplitude, more regionally and seasonally confined, and less coherent across models and observations. As a result, their global-scale contributions, although important, are secondary compared to ENSO.

Therefore, while we acknowledge the broader issue raised by the reviewer as an important avenue for future research, we believe it is beyond the scope of the present study. Our objective here is to isolate and clarify the ENSO pathway as the leading driver of tropical–global SST teleconnections. We have revised the manuscript to make this scope explicit and to highlight that our focus on ENSO does not preclude the possibility of similar mechanisms operating in other tropical modes.

Requests for additional analyses:

4. In the analysis of maximum R2 value, it is not clear which values are related each other and which are independent, so it would help to understand the mechanism if a map of the lag "tau" at the maximum absolute value is drawn together. In MME, is there uncertainty in the spatial distribution of the lag "tau"?

Ans) We quantify ensemble phase agreement for τ using the mode across CMIP6 34 models at each grid point (Fig. R2-2). We then count how many models fall within plus-or-minus one and plus-or-minus two phases of that center. The ocean fraction where at least half of the models agree is ~30% for the ±1 month criterion and ~60% for the ±2-month criterion, indicating substantial model dependence—regional coherence in some basins, but considerable spread elsewhere. Figure R2-3 further shows τ for CESM1 and the observations; the scatter marks regions where CESM1 lies within the ±2-month criterion relative to observations. Agreement is strong in some areas and weaker in others. Nevertheless, even without exact uniformity in τ, broad phase coherence is evident, and the strengthening of the ENSO–SST teleconnection remains robust across models (Extended Data Figs. 2 and 3). This robustness reflects that our results are insensitive to the precise lag choice—the amplification persists across reasonable τ windows. (See also our response to Specific Comment L81–L82)

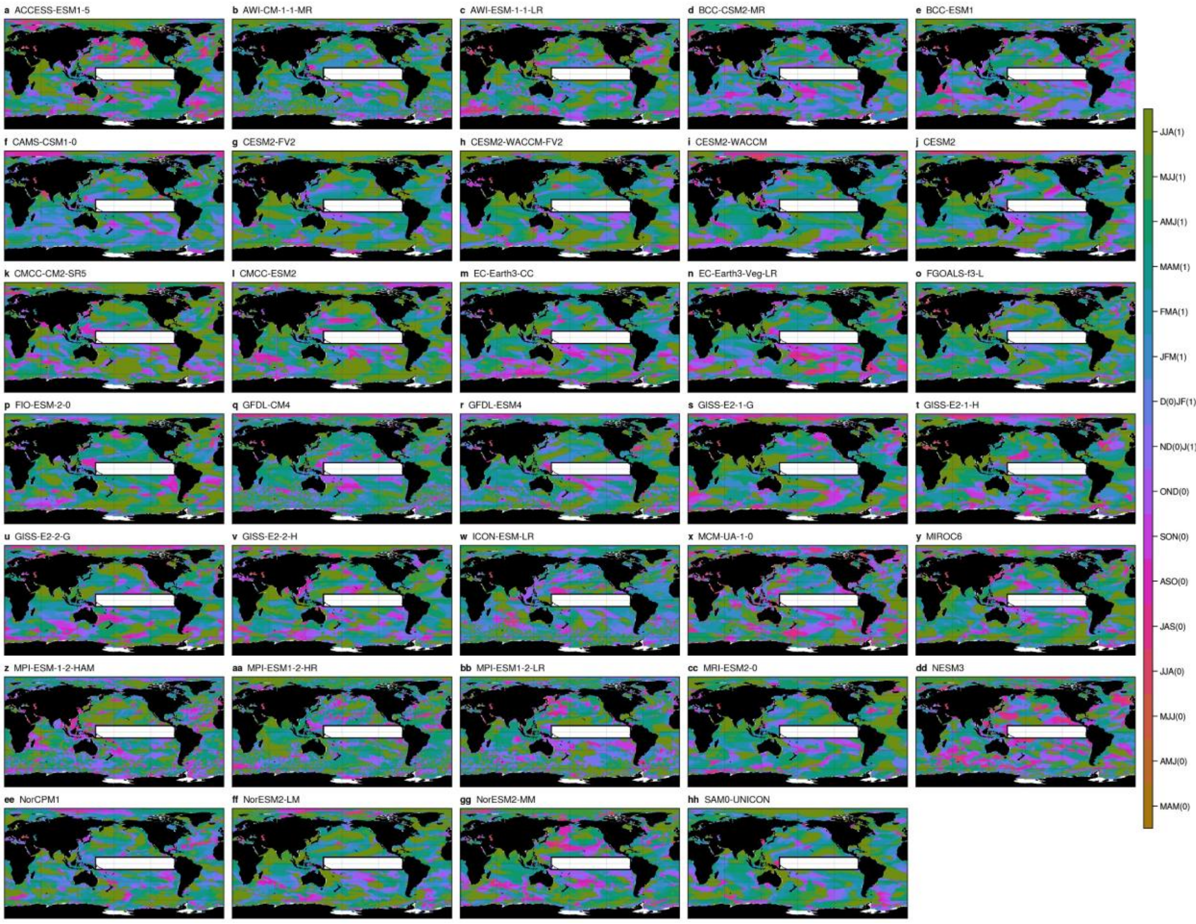

Fig. R2-2 | τ in each CMIP6 models. Maps of τ in each CMIP6 models.

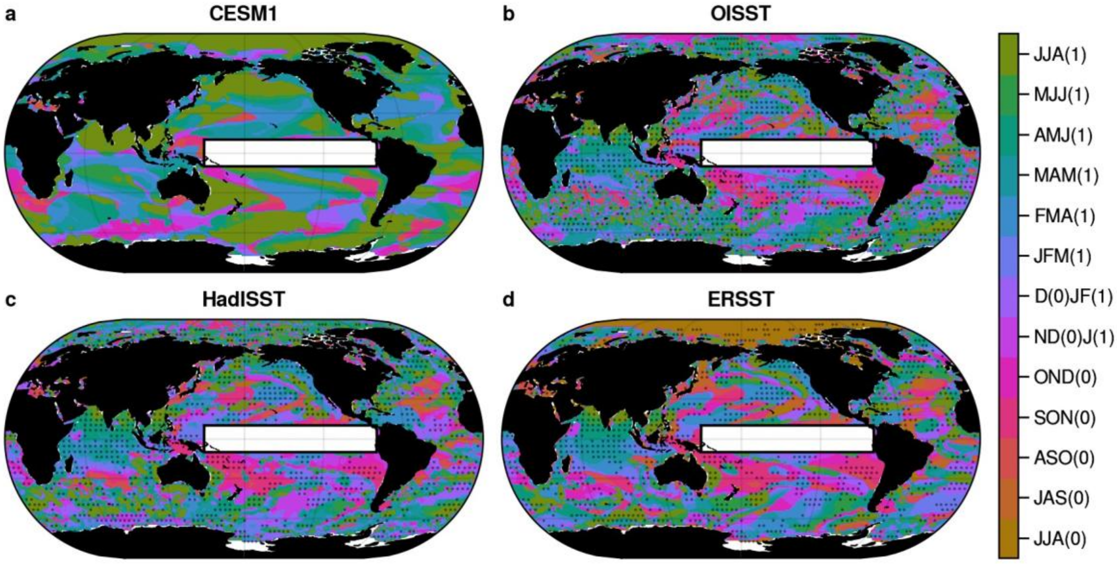

Fig. R2-3 | Maps of τ in observation. In **a** CESM1, **b** OISST, **c** HadISST and **d** ERSST τ, respectively. Stippling in **b-d** indicates corresponding to "$\tau \pm 2$" of CESM1. The white box shows the Equatorial Pacific region, to exclude El Niño SSTA itself.

5. In the analyses, MAM(0) is used as the baseline and the difference from it is analyzed to judge the maximum R2 value and conduct the mixed layer heat budget analysis. But the spatial distribution of the maximum R2 value or the heat budget terms must depend not only on the values at the time lag "tau" but also on the pattern at MAM(0). How much of impacts do this baseline values have?

Ans) To assess baseline sensitivity, we repeated the analysis with anchors shifted by ±2 months around MAM(0)—JFM(0), FMA(0), AMJ(0), and MJJ(0)—and recomputed the PD to 2100 change in R^2, with τ evaluated relative to each anchor. As shown in Figure R2-4, the spatial patterns are essentially unchanged (pattern correlation > 0.9), indicating that our results are insensitive to the baseline choice and that baseline effects are negligible.

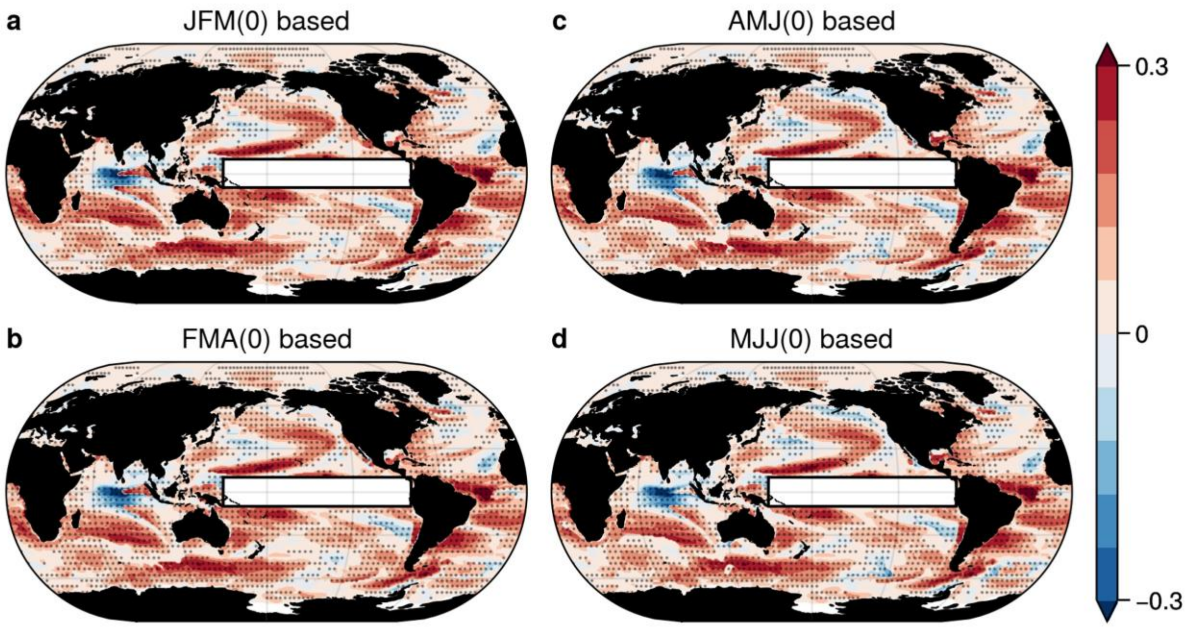

Fig. R2-4 | Changes in ENSO impacts on global SST based on different baseline. a JFM(0) based, **b** FMA(0) based, **c** AMJ(0) based, and **d** MJJ(0) based calculated changes in R^2 from the PD to 2100 with different τ in CESM1. Stippling indicates regions that are statistically significant at the 95% confidence level using the bootstrap test.

6. In the Eq.1, not only the SFC term but also the other budget terms (the advection terms, diffusion term) should be shown.

Ans) We are sorry for the ambiguity. We did not diagnose the model's full mixed layer temperature tendency $\partial T_m/\partial t$ nor close the complete budget. Instead, we used the mixed layer heat budget as a diagnostic framework and quantified only the surface flux-driven component of the ENSO-related SSTA by time-integrating the surface flux term. The ocean dynamical term is difficult to be calculated due to the availability of the necessary oceanic variables. Therefore, the residual ($SST_{TOT} - SST_{SFC+MLD}$) collects all non-surface flux processes such as horizontal/vertical advection, entrainment process, and diffusion. We have revised the Methods to explicitly state this and replaced phrases suggesting "SST tendency" with wording "surface flux contribution to the ENSO-driven SSTA". We have also added clear sentences.

(L306-313): We calculated the surface flux-induced SSTA in diagnostic framework, based on the following mixed layer heat budget equation:

$$\frac{\partial T_m}{\partial t} = \frac{Q_{net}}{\rho_0 C_p h} + Res, \quad (1)$$

where T_m is the mixed layer temperature, Q_{net} is net surface flux (positive into the ocean), ρ_0 (1027 kg m^{-3}) is the reference density of seawater, C_p (3985 J kg^{-1} K^{-1}) is the specific heat of seawater at constant pressure. We only used surface flux term and calculate the surface flux contribution to ENSO-driven SSTA. The Res mainly represents contributions from ocean dynamical processes such as horizontal/vertical advection, entrainment, and diffusion.

7. To understand the differences among MME models in the maximum R2 values and wind speed responses, please add figures of the maximum R2 values and wind speed regressions for each model to the Extended Data Figures.

Ans) We have added the Extended Data Figure with the change in maximum R^2 values and wind speed responses, respectively.

Fig. R2-5 | The changes in the maximum R^2 values in each CMIP6 models. A-hh The difference in maximum R^2 between SSTA and DJF Niño3.4 in each CMIP6 models.

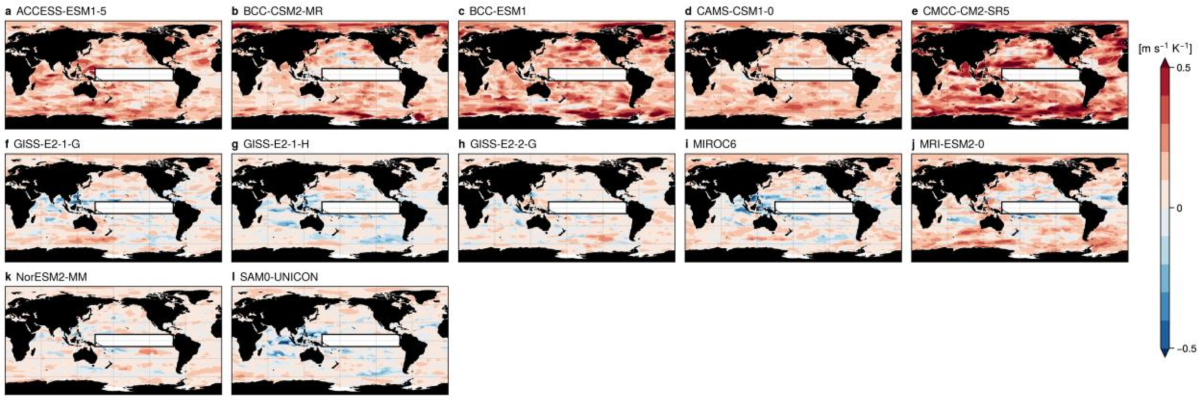

Fig. R2-6 | The changes in surface wind speed responses in each CMIP6 models. A-l The difference in absolute maximum of surface wind speed regressed onto DJF Niño3.4 from MAM(0) to JJA(1) between PD to 2100.

Specific comments:

L32-L42: Shifts in the position of the westerly jets due to global warming should also be important in changing the teleconnection pattern. Please add this in the text as it is an important factor in understanding the process of this study.

Ans) We have added a statement on the role of westerly jet.

(L41-43): Moreover, the changes in position and strength of westerly jet under greenhouse warming are expected to modulate these teleconnections by altering the midlatitude waveguide[21,22].

L81-L82: Is the time lag "tau" also similar at each grid point between CESM1 LE and the observations?

Ans) Figure R2-3 depicts τ (peak-lag) maps for CESM1 and for each observational dataset. Their spatial patterns are similar, but clear differences are also found in some regions. The differences might arise from the systematic biases in ENSO teleconnection of the climate models. In order to check whether the systematic biases in τ are critical for the main arguments of the present study, we calculated R^2 for each season and their changes under global warming.

Figure R2-7 and R2-8 show season-fixed changes in R^2—JJA(0), SON(0), DJF(1), MAM(1), and JJA(1) in CESM1 and CMIP6 multi-model mean, respectively. Across all five seasons both the CESM1 and CMIP6 multi-model mean indicate a consistent increase in R^2, demonstrating that our conclusions are not sensitive to the τ. Uncertainty is summarized by stippling in Fig. R2-8, where more than 70% of models agree on the sign of the R^2 change. Together, these results show that the strengthening is robust in all lead-lag time rather than tied to a particular τ.

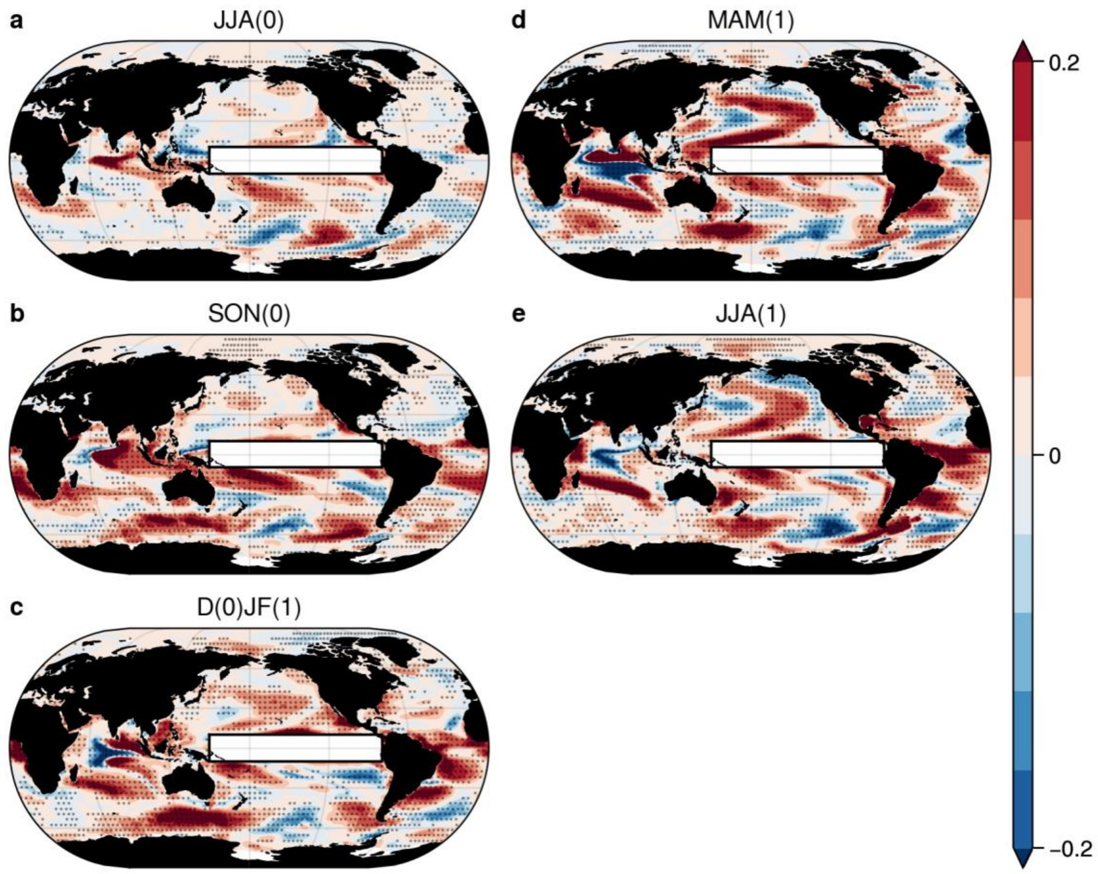

Fig. R2-7 | The changes in R^2 in each lead-lag season in CESM1. a-e CESM1 difference in R^2 between 1pctCO2 2085-2115 and present-day, evaluated at fixed seasons: **a** JJA(0), **b** SON(0), **c** D(0)JF(1), **d** MAM(1) and **e** JJA(1). Stippling indicates statistically significant at the 95% confidence level using the bootstrap test.

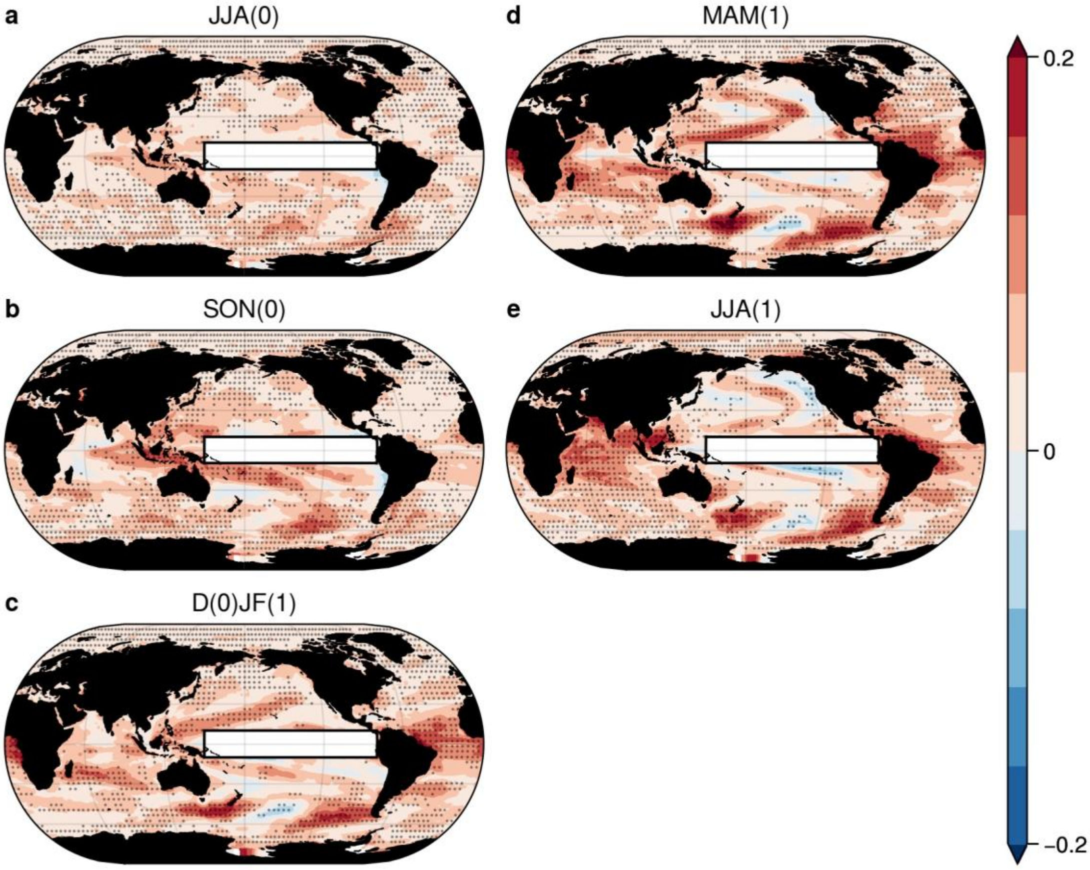

Fig. R2-8 | The changes in R^2 in each lead-lag season in CMIP6. a-e CMIP6 multi-model mean difference in R^2 between 1pctCO2 2085-2115 and historical, evaluated at fixed seasons: **a** JJA(0), **b** SON(0), **c** D(0)JF(1), **d** MAM(1) and **e** JJA(1). Stippling indicates more than 70% of models agree on the sign of R^2 change.

L90-L91: What are the reasons for the weakening of the ENSO impact in the tropical Indian Ocean?

Ans) To address the reviewer's comments, Figure R2-7 examines the equatorial Indian Ocean and compares four diagnostics—SST_{TOT}, $SST_{SFC+MLD}$, SST_{SFC}, and SST_{MLD}—together with time series of SSTA regressed onto the DJF Niño3.4 SSTA. The gap between SST_{TOT} and $SST_{SFC+MLD}$ indicates a substantial contribution from ocean dynamics in this region. Consistent with previous studies, El Niño is linked to Indian Ocean variability through two phases: during the growth phase, in addition to atmospheric heat-flux effects, dynamical processes (thermocline shoaling/upwelling and associated circulation changes) strengthen a Bjerknes feedback (Bjerknes, 1969), fostering the development of the Indian Ocean Dipole (IOD) and enhancing cooling in the eastern equatorial basin (Saji et al., 1999); during the decay phase, surface heat-flux anomalies favor the Indian Ocean Basin Mode (IOBM) and yield basin-wide warming (Klein et al., 1999; Cai et al., 2019).

Because our primary decomposition isolates the surface-flux pathway, the growth-phase dynamical cooling is not fully captured, implying that our thermodynamic estimate alone cannot fully explain SST evolution. This interpretation is supported by the diagnostics: SST_{TOT} shows stronger cooling than $SST_{SFC+MLD}$, consistent with an enhanced dynamical contribution, whereas SST_{SFC} indicates that the surface-flux pathway itself strengthens under warming. Taken together, these results suggest that the overall El Niño influence on the equatorial Indian Ocean intensifies, but the decay-phase warm SST anomaly becomes weaker in 2100. This compensation explains why the signal over the equatorial Indian Ocean appears muted (and locally cooler) despite the increased ENSO impact.

Bjerknes, J. ATMOSPHERIC TELECONNECTIONS FROM THE EQUATORIAL PACIFIC. *Monthly Weather Review* **97**, 163–172 (1969).

Cai, W. *et al.* Pantropical climate interactions. *Science* **363**, eaav4236 (2019).

Saji, N. H., Goswami, B. N., Vinayachandran, P. N. & Yamagata, T. A dipole mode in the tropical Indian Ocean. *Nature* **401**, 360–363 (1999).

Klein, S. A., Soden, B. J. & Lau, N.-C. Remote Sea Surface Temperature Variations during ENSO: Evidence for a Tropical Atmospheric Bridge. (1999).

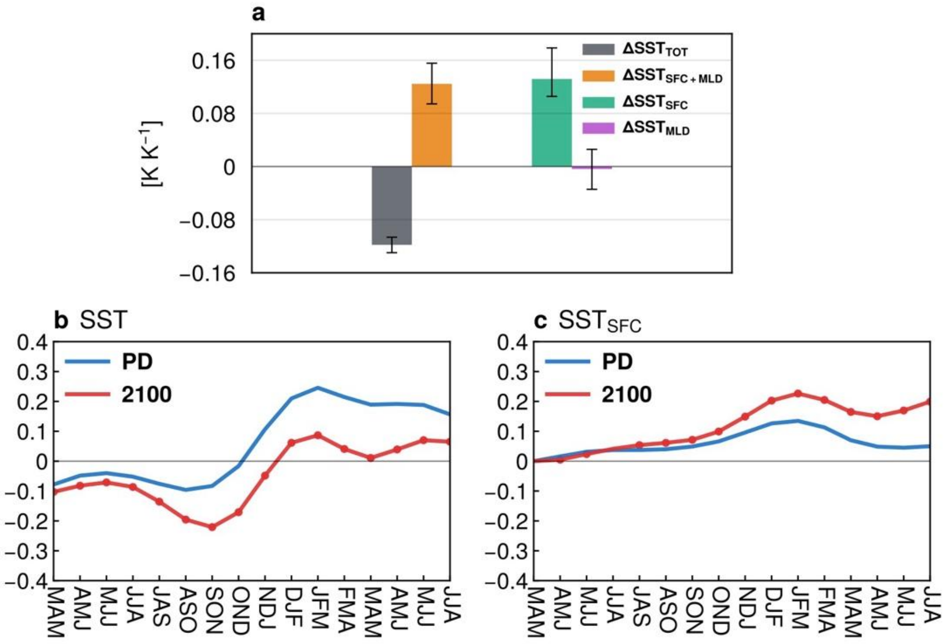

Fig. R2-7 | The mechanisms of decrease in El Niño impact on Indian Ocean SST variability. a Same as Extended Fig. 5a for Equatorial Indian Ocean (60°E–85°E, 10°S–5°N). **b** Temporal evolution of SSTA regressed onto DJF Niño3.4 SSTA from MAM(0) to JJA(1), during PD (blue line) and the 2100 period (red line) for Equatorial Indian Ocean. **c** Temporal evolution of SSTA changed by the only El Niño-induced surface flux (conducted with SFC regressed on DJF Niño3.4 SSTA). Red dots indicate statistically significant at the 95% confidence level using the bootstrap test.

Please specify the number of ensembles in the CMIP6 1pctCO2 experiments for each model.

Ans) Revised.

(L274-275): In addition, 34 models in the CMIP6 pre-industrial and 1pctCO2 scenarios are employed, using one ensemble member per model for each experiment.

L115: Before the explanation of "MLD", the subscript representation of "SFC+MLD" appears. At this point, there is no explanation of the difference between "SFC+MLD" subscripts, "SFC"-only subscripts, and "MLD"-only subscripts, which is confusing, so please revise the order of the explanations.

Ans) Revised.

(L113-126): We adapted the mixed-layer heat budget equation to decompose the contributions to the enhanced El Niño impacts. Previous studies have identified surface flux (SFC; positive into the ocean) as a primary driver of SST responses to ENSO[25,36,37]. To quantify the contribution of the SFC, we first define $SST_{SFC+MLD}$ as the time-integrated the surface flux-related term of the equation, which is determined by (i) El Niño-induced surface flux anomaly and (ii) climatological mixed layer depth (MLD, see Methods for details). Figure 2a shows that the magnitude of the $SST_{SFC+MLD}$ is larger than SST_{TOT} in both PD and 2100, possibly due to the damping role of the ocean dynamics. These results suggest that the SFC is a primary driver inducing ENSO-driven global SSTA at least on a global average. Additionally, the changes in $SST_{SFC+MLD}$ between PD and 2100 are comparable to the change in SST_{TOT}, indicating that the amplified El Niño impacts can be attributed to anomalies induced by SFC.

To separate the mechanism, we decompose $SST_{SFC+MLD}$ into (i) SST_{SFC}, which holds MLD fixed at its PD climatology, and (ii) SST_{MLD}, which holds the surface flux anomaly (SFC anomaly regressed onto DJF Niño3.4) fixed at its PD value (see Methods for details).

13) L284: Why did you use MAM(0) as the baseline? Why were DJF(0) and JFA(0) skipped?

Ans) We anchor at MAM(0) because it marks the onset of El Niño growth, whereas D(-1)JF(0) (mature), JFM(0) and FMA(0) (transition) emphasize non-onset phases. An onset baseline reduces phase-mixing between peak and decay and focuses the timing metric on teleconnection development. We estimate τ within ±2 months of the anchor and compare PD vs. 2100. Figure R2-3 shows that sensitivity tests with adjacent anchors yield near-identical spatial patterns: pattern correlations with the MAM(0) fields are 0.93 (JFM(0)), 0.97 (FMA(0)), 0.97 (AMJ(0)), and 0.94 (MJJ(0)). Thus, our conclusions are robust to the baseline; D(-1)JF(0), JFM(0), and FMA(0) were not used to avoid phase-mixing outside the onset window.

L484 (Fig. 3 caption): "g" -> "d"

L486 (Fig. 3 caption): "d-e" -> "e-f"

L487 (Fig. 3 caption): "f" -> "g"

Ans) Revised.

Response to Reviewer #4

The manuscript investigates the changes in ENSO-related SST variability under global warming based on climate models. It is a very interesting work suggesting that per-unit ENSO SST anomalies could induce amplified global-scale SST feedback responses under global warming scenarios. The results carry significant implications for improving climate projections of future variability. Through heat budget analysis using model data, the manuscript indicates that intensified ENSO-related wind speed and air-sea humidity difference are the main factors contributing to the enhanced SST anomaly responses. To address distinct climate regimes for different regions, the manuscript conducts diagnostics on four selected regions exhibiting specific atmospheric feedback responses.

The study is well designed and the manuscript is clearly written, guiding the reader towards its main conclusions. The methods section and the Extended file cover necessary details on datasets, analysis and experiments.

We appreciate the reviewer's encouraging and constructive comments. The reviewer's comments were fully reflected in the revised manuscript, and we carefully checked and revised the manuscript. Our responses to the specific comments are as follows:

Comments:

1. I guess my main comment/question lies in why could the same unit of ENSO SST anomalies lead to a stronger wind feedback through intensified atmospheric convection in the 2100 scenarios, compared with the PD simulation as showed in Figure.3. In other words, why could the same magnitude of ENSO SSTA induce stronger atmospheric convection feedback in a warming world? Is the cause attributed to changes in the atmospheric mean states affecting convective processes, an acceleration in atmosphere feedback establishment, or other factors? I guess a deeper analysis or discussion would greatly improve the comprehension of the underlying physical mechanisms in this manuscript.

Ans) Thanks for the insightful comment. The intensified precipitation responses to ENSO-related equatorial Pacific SST anomalies under global warming have been demonstrated in previous studies, which provide plausible physical mechanisms. First, atmospheric warming increases column water vapor approximately at the Clausius–Clapeyron rate, so that a given SST anomaly induces stronger precipitation and diabatic heating (Yun et al., 2020; Huang et al., 2015). Second, El Niño–like mean state changes promote an eastward extension of ENSO-related convection anomalies (Power et al., 2013; Cai et al., 2014; Kug et al. 2010; Geng et al. 2023). As a result, the same SST anomaly induces a larger atmospheric response—manifested as stronger convective heating and circulation changes under warming (Hu et al., 2021). To explicitly reflect these mechanisms, we revised the results section as follows:

(L165-176): The intensified El Niño–related wind responses are likely linked to enhanced convective responses driven by ENSO SST forcing. As shown in Fig. 3d, positive precipitation anomalies over the central and eastern Pacific become stronger and extend farther eastward under greenhouse warming. Such intensified precipitation responses have been documented in previous studies, which proposed plausible physical mechanisms[42]. First, atmospheric warming increases column water vapor at approximately the Clausius–Clapeyron rate, so that a given SST anomaly produces stronger precipitation and diabatic heating[16,43]. Second, El Niño–like mean state changes favor an eastward extension of ENSO-related convection anomalies[13,14,18,44]. Consequently, the same El Nino-related SST anomaly induces a larger atmospheric response—manifested as stronger convective heating and circulation changes under warming[33]. This intensified atmospheric circulation, in turn, leads to stronger anomalous surface wind speeds, thereby modulating evaporation through enhanced air–sea interaction.

Yun, K.-S. et al. Increasing ENSO–rainfall variability due to changes in future tropical temperature–rainfall relationship. *Commun Earth Environ* **2**, 1–7 (2021).

Huang, P. & Xie, S.-P. Mechanisms of change in ENSO-induced tropical Pacific rainfall variability in a warming climate. *Nature Geosci* **8**, 922–926 (2015).

Power, S., Delage, F., Chung, C., Kociuba, G. & Keay, K. Robust twenty-first-century projections of El Niño and related precipitation variability. *Nature* **502**, 541–545 (2013).

Cai, W. *et al.* Increasing frequency of extreme El Niño events due to greenhouse warming. *Nature Clim Change* **4**, 111–116 (2014).

Kug, J.-S., An, S.-I., Ham, Y.-G. & Kang, I.-S. Changes in El Niño and La Niña teleconnections over North Pacific–America in the global warming simulations. *Theor Appl Climatol* **100**, 275–282 (2010).

Geng, X., Zhao, J. & Kug, J.-S. ENSO-driven abrupt phase shift in North Atlantic oscillation in early January. *npj Clim Atmos Sci* **6**, 80 (2023).

Hu, K., Huang, G., Huang, P., Kosaka, Y. & Xie, S.-P. Intensification of El Niño-induced atmospheric anomalies under greenhouse warming. *Nat. Geosci.* **14**, 377–382 (2021).

Specific comments:

I suggest the manuscript could include some analyses on the changes in ENSO amplitude (PD .vs. 2100) from CESM1 runs. On this basis, the manuscript further examines the global SST variations induced by per unit amplitude of ENSO SSTA—even though this does not fundamentally alter the work's main conclusions.

Ans) Thanks for the helpful suggestion. We agree that assessing the total ENSO influence on SST—rather than only the per-unit amplitude response—is important. We quantify ENSO's overall SST impact as the product of (i) the sensitivity of SST to a unit-strength ENSO event (the regression coefficient, β) and (ii) ENSO amplitude (the standard deviation of the ENSO index, σ). Following the regression-based decompositions of Lin et al. (2024) and Wu et al. (2021), we separate the projected change in this total impact into (a) a non-amplitude term linked to changes in β, (b) an amplitude term linked to changes in σ, and a small second-order residual. The formal definitions and implementation details are provided in the Extended Data Text.

Decomposition of changes in El Niño impacts on SSTA

The changes in El Niño impacts on SST is calculated as follows:

$$Y' = \beta \times \text{Niño3.4} + Res_1, \quad (S1)$$

where Y' is SSTA(τ), β is the regression coefficient, which indicates ENSO-induced SSTA, and Res_1 is the residual. Unit of β is K per 1K of DJF Niño3.4 SSTA (DJF Niño3.4). We used the $|\beta|$ as a representation of ENSO impacts on SSTA.

Following the Lin et al. (2024) and Wu et al. (2021), SSTA(τ) regression is also conducted with DJF Niño3.4$_{std}$, which represent standardized Niño3.4 SSTA as follows:

$$\text{Niño3.4}_{std} = \text{Niño3.4}/\sigma$$
$$Y' = \beta_{std} \times \text{Niño3.4}_{std} + Res_2, \quad (S2)$$

where σ is the standard deviation of DJF Niño3.4, β_{std} is the regression coefficient indicating ENSO-induced SSTA per one-standard deviation of ENSO, and Res_2 is the residual. β_{std} consists of two influences: (i) non-amplitude factor (the regression coefficient, β) and (ii) ENSO amplitude factor (the standard deviation of the ENSO index, σ). Since the $|\beta_{std}| \approx |\beta| \times \sigma$ from Eq. S2 and S3, decomposition of these two factors is calculated as follows:

$$\Delta|\beta_{std}| = \Delta|\beta| \times \sigma_{PD} + |\beta_{PD}| \times \Delta\sigma + Res_3, \quad (S3)$$

where Δ means difference between 2100 and PD periods, the subscript PD indicates the PD period, Res_3 is the residual term. Using Eqs. S2 and S3, we decompose the contribution of non-amplitude and amplitude factor.

Applying this framework, we found that the increase in ENSO's SST influence is dominated by the non-amplitude component. In CESM1, the non-amplitude pathway explains ~64% of the total increase, while amplitude changes account for ~32% (with a small residual). In the CMIP6 multi-model mean, the dominance of the non-amplitude term is even clearer (~76%), with amplitude contributing ~20% and a minor residual. These results indicate that background-state and teleconnection-related changes in SST sensitivity to a unit ENSO amplitude play the leading role in amplifying ENSO's overall SST impact, consistent with our main finding that strengthened El Niño-induced wind-speed anomalies and enhanced climatological air-sea humidity contrast drive the projected amplification. The relatively modest amplitude contribution in the CMIP6 mean also aligns with the interpretation of Extended Data Figure 15.

Consistent with this interpretation, Figures R3-1 a and e show that the per-unit-amplitude impact on SST strengthens in both CESM1 and CMIP6. To make the total-impact perspective explicit, we have added Extended Data Figure 14, which maps the total change and its decomposition (non-amplitude vs. amplitude), and we discuss these contributions in the revised Discussion. We also reference Extended Data Figure 15 when summarizing the amplitude component and its comparatively modest role in the CMIP6 mean.

Overall, these additions clarify that while ENSO amplitude does change, the leading driver of the projected increase in ENSO's SST influence is the enhanced sensitivity—consistent with our main result that strengthened El Niño-related wind-speed anomalies and an enlarged climatological air–sea humidity contrast intensify the thermodynamic pathway under warming.

(L237-245): To quantify ENSO's total SST influence, we decomposed it into a non-amplitude term and an amplitude term, following regression-based approaches (Extended Data Text). The results show that the increase is dominated by non-amplitude component changes—~64% in CESM1 and ~76% in the CMIP6 multi-model mean—while amplitude accounts for ~32% and ~20%, respectively; importantly, even models with reduced ENSO amplitude[54–56] show a net increase because atmospheric and oceanic sensitivity strengthens (Extended Data Fig. 15 and 16). In summary, background-state/teleconnection changes dominate, but amplitude changes are not negligible.

Lin, S., Dong, B. & Yang, S. Enhanced Impacts of ENSO on the Southeast Asian Summer Monsoon Under Global Warming and Associated Mechanisms. Geophysical Research Letters 51, e2023GL106437 (2024).

Wu, R., Chen, W., Wang, G. & Hu, K. Relative contribution of ENSO and East Asian winter monsoon to the South China Sea SST anomalies during ENSO decaying years. Journal of Geophysical Research: Atmospheres 119, 5046–5064 (2014).

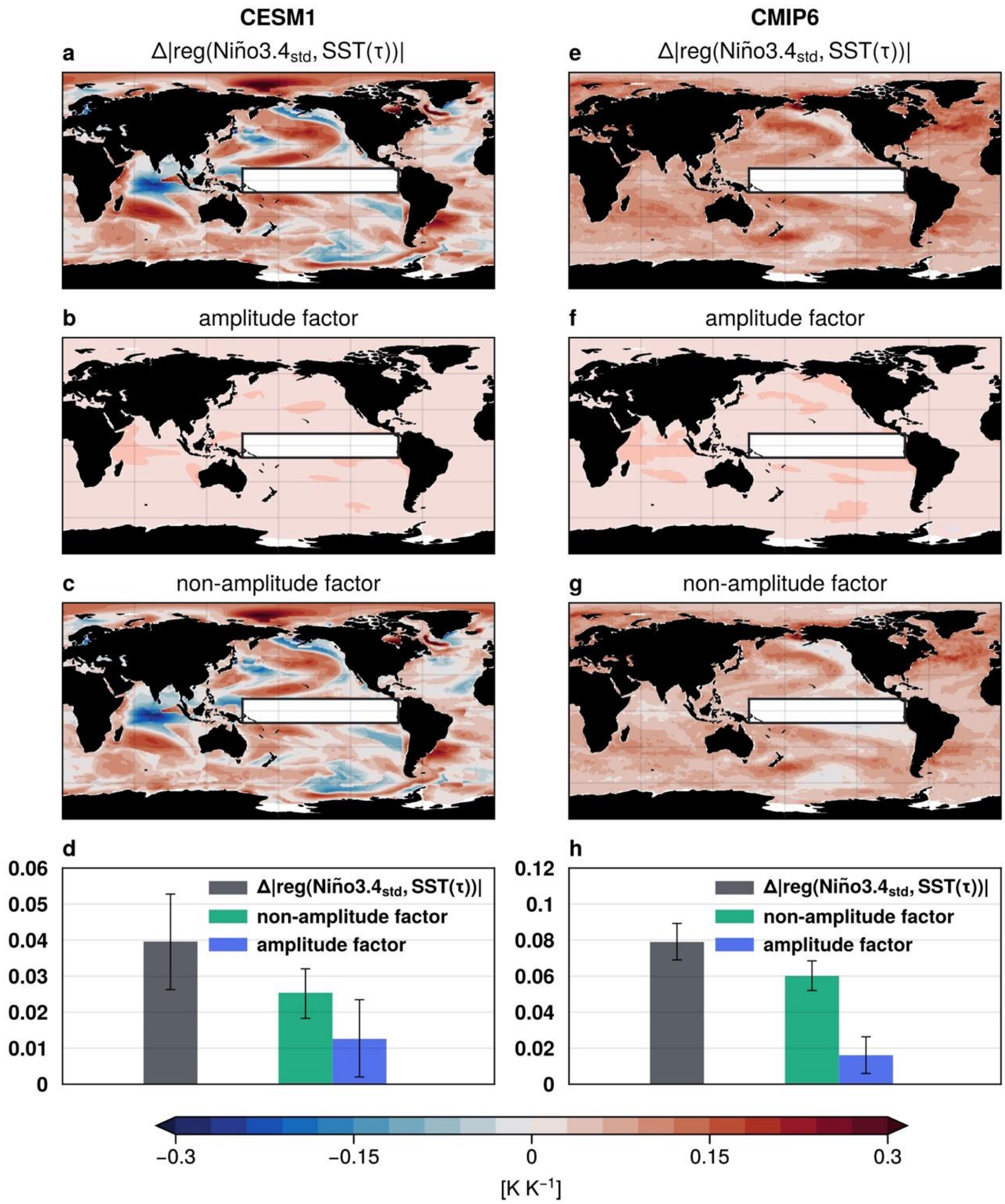

Fig. R3-1 | Decomposition of the changes in ENSO impacts on SST. a The changes in absolute values of SSTA(τ) regressed onto DJF Nino3.4 SSTA from the PD period to 2100. The contribution of **b** amplitude factor and **c** non-amplitude factor. **d** Global mean of (1) the changes in absolute values of SSTA(τ) regressed onto DJF Nino3.4 SSTA from the PD period to 2100, (2) non-amplitude factor, and (3) amplitude factor. **e-h** are as the same as a-d (respectively) but CMIP6 multi-model mean.

Do any grid points exhibit τ values preceding the ENSO peak (e.g. Atlantic Niño (JJA0) could trigger an ENSO (D0JF1) event)? If present, would this phase-leading relationship necessitate larger-amplitude SSTA forcing to produce equivalent ENSO SST anomaly intensities?

Ans) Figure R3-2 shows grid points where τ precedes the ENSO peak more than three months (JJA(0)–SON(0)); these occupy only 6.1% of the analyzed area. In addition, most months of the 6.1% were SON(0), close to the ENSO mature season. Thus, while precursor SSTA (e.g., an Atlantic Niño) can occur, its spatial footprint is small. Consequently, we do not view the 2100 increase in ENSO-related SST variability as requiring larger-amplitude precursor SSTA to achieve comparable DJF ENSO anomalies. Any phase-leading influence is likely minor at the basin scale.

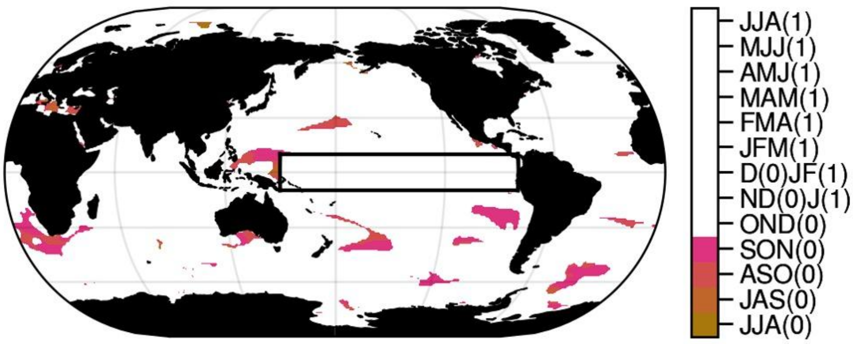

Fig. R3-2 | Regions where τ leads the ENSO peak (JJA(0)-SON(0)) in CESM1. Map of grid points where the period with the most significant deviation in correlation from the MAM(0) baseline (τ) is JJA(0), JAS(0), ASO(0), and SON(0).

According to Figure.1, the explainable variance R2 of SST in 2100 simulation is stronger than that in PD. Does this finding suggest a strengthening of the linear response component in ENSO's climatic impacts in 2100 due to more stable atmospheric stratification?

Ans) We appreciate the question. We constructed separate composites of global SST anomalies for El Niño and La Niña events for the PD and for 2100, and we further examined the change in their absolute values (|2100|–|PD|; Fig. R3-3). Events are defined by DJF Niño-3.4 SSTA exceeding ±1 standard deviation (≥+1σ for El Niño; ≤−1σ for La Niña), and the temporal alignment follows the same protocol as the maximum R^2 analysis (see Methods for details). Here, however, we analyze composite amplitudes rather than correlations. Figure R3-3 shows widespread increases even in a metric that includes nonlinear responses, indicating a stronger total ENSO impact, not merely greater linearity. Although the changes are asymmetric between El Niño and La Niña, both phases exhibit coherent intensification, implying that the underlying dynamical pathways have strengthened. Accordingly, as we discussed before, we attribute the higher R^2 primarily to stronger ENSO-driven deep convective heating (i.e., a stronger anomalous circulation) and an enhanced air–sea humidity contrast that increases latent heat flux efficacy, rather than more stable atmospheric stratification.

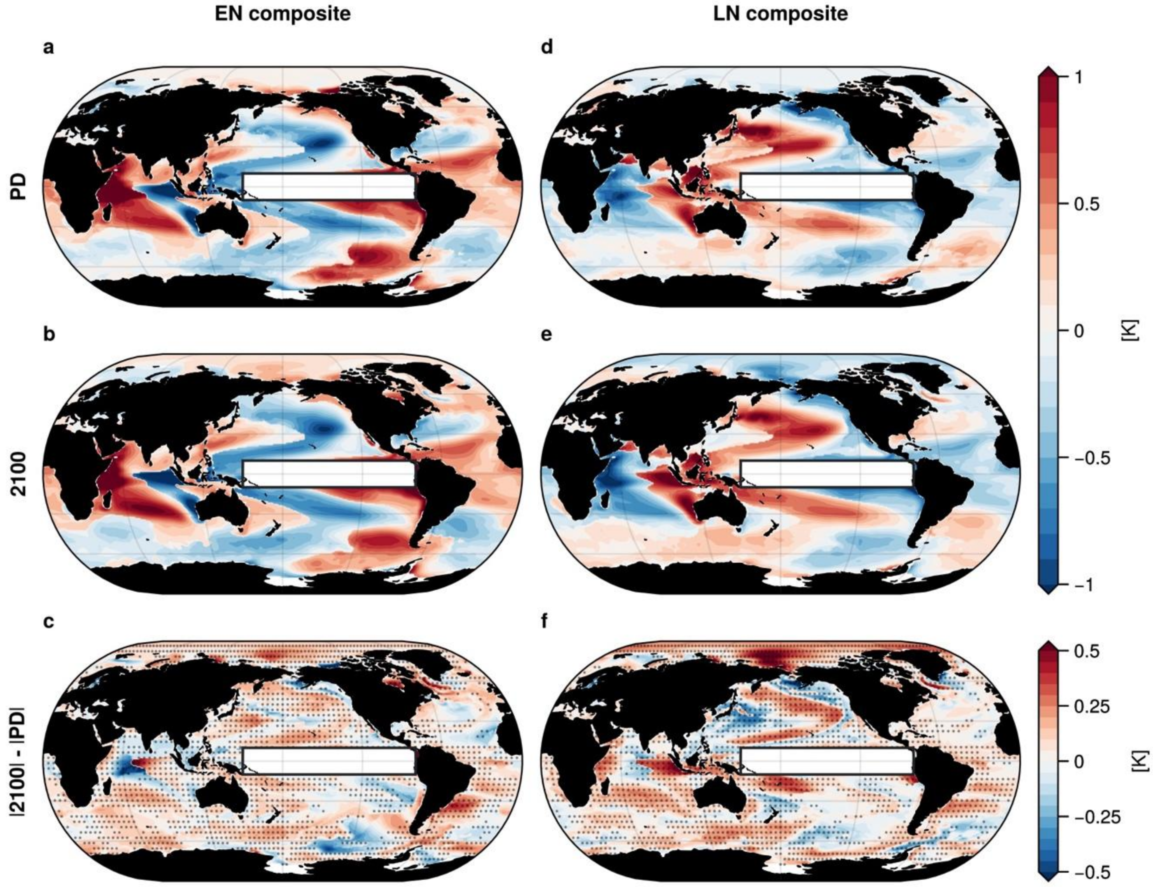

Fig. R3-3 | Changes in El Niño and La Niña impacts on SST. a-c El Niño composites for PD, 2100, and the change in absolute magnitude (|2100|-|PD|), taking the absolute maximum over the JJA(0)–JJA(1). **d-f** As in a-c but for La Niña. Stippling denotes regions where the change in absolute amplitude is statistically significant at the 95% confidence level using a bootstrap test. The white box marks the equatorial Pacific region to exclude ENSO SST itself.

L33: Suggest using "anomalies" instead of "anomaly".

Ans) Revised from "anomaly" to "anomalies"

There appears to be an inconsistency in Figure 3, where the annotations for panels (e) and (g) seem to be inadvertently swapped.

Ans) Figure 3 caption has been revised accordingly.

In Figure 4b-e, what does the hatches between the blue and red lines represent?

Ans) Revised the caption of Figure 4.

(L537-540): Vertical line marks τ (See Methods for details). The hatches shows the net difference between the 2100 and PD ENSO-induced latent heat flux curves (starting at the last moment before τ when the two curves are equal and ending at τ). A hatched area indicates an enlarged net heat uptake/loss during that window.

In Figure 4b-e, unlike the SST results, the temporal evolution of regression coefficients for latent heat flux appears to exhibit distinct peak timings (except SIO). Does this suggest an alteration in air-sea interaction processes between PD and 2100?

Ans) While the differing peak months of the latent heat flux regressions could indicate changes in air–sea coupling in principle, we interpret them as modest phase shifts of the same basic coupling mechanism (set by wind speed and air-sea humidity contrast) in a warmer mean state. Warming shifts the seasonal background circulation and humidity gradient, enabling the latent heat flux maximum to occur about 1 month earlier or later. In contrast, SST integrates these fluxes; therefore, its peak remains the same with present-day despite the latent heat flux maximum timing shift. Therefore, the interaction does not occur in a fundamentally different way, which does not affect our conclusions.

There are differences in the chosen time window for τ (L285: JJA(0)-JJA(1); L314: MAM(0)-JJA(1)) in Methods.

Ans) Thank you for pointing this out. The difference is intentional, and we have revised the Methods to state it explicitly. Specifically, τ is an SST-based quantity defined as the month with the maximum explained variance within JJA(0)–JJA(1) (relative to MAM(0)), reflecting the usual post-spring peak of the teleconnection. By contrast, the forcing peak (wind speed regression) is identified as the month with the largest absolute regression magnitude over MAM(0)–JJA(1), allowing the forcing to lead τ. We revised the Methods as following for clarity, explicitly stating the two search windows and the reasoning behind them.

(L327-330): For the maximum wind speed forcing, we identify the month with the largest absolute regression onto DJF Niño3.4 SSTA within MAM(0)-JJA(1) (including MAM(0)-MJJ(0)). We allow this to differ from τ because surface flux forcing generally precedes the SST response, so its timing may lead τ.

Response to Reviewers #1:

The authors have satisfactorily addressed all my previous concerns, and I recommend the manuscript for acceptance.

Response to Reviewers #2 & #3:

Reviewers #2

I co-reviewed this manuscript with one of the reviewers who provided the listed reports. This is part of the Nature Communications initiative to facilitate training in peer review and to provide appropriate recognition for Early Career Researchers who co-review manuscripts.

Reviewers #3

I sincerely appreciate the authors' conscientious and thoughtful responses. While I believe that many of the points have been addressed appropriately, I feel that the response regarding the part that I find most questionable—the understanding of the process—has not been explained sufficiently.

Comments:

My main concern is that, regardless of whether the forcing originates from ENSO, CP, or EP, the maximum R2 pattern and the wind speed response appear quite similar. This suggests that the phenomenon may no longer be specific to ENSO. By focusing exclusively on ENSO, I am concerned that the authors may be overlooking a more fundamental and general process that does not depend on ENSO.

Ans) We agree with the reviewer that our results suggest the operation of a more general tropical-forcing mechanism. Our additional analyses for the Indian and Atlantic Oceans indeed support this broader interpretation. Nevertheless, in this study we intentionally focus on ENSO, because it is by far the strongest, most spatially extensive, and most robust source of interannual tropical SST forcing and global teleconnections in both observations and models. While the same physical processes may apply to other tropical modes, their impacts are weaker and more regionally confined. We therefore believe that framing the analysis around ENSO provides the clearest and most relevant context, while we explicitly acknowledge in the Discussion that the underlying mechanism is likely applicable to tropical SST forcing more generally.

In Fig. R2-1, the authors state that the agreement between panels (a, b, c), and d is less than 20%; however, to my eye, the pattern correlations appear to be reasonably high. I do not think perfect coincidence is necessary, so I recommend examining the comparisons more carefully.

Ans) Thanks for the thoughtful suggestion. We also agree with the reviewer. Following the reviewer's recommendation, we calculated the difference in the timing of peak variance (in months) between ENSO-induced windspeed variability and climatological wind variability (Fig. R3-1). As noted by the reviewer, the peak-month difference is within ±1 month for more than 50% of the grid points, indicating that the two largely share their maximum variance within the same season. Given the strong seasonality of internal atmospheric variability (e.g., winter in the extratropics), the ENSO-forced wind response can be amplified during these periods. More generally, the magnitude of ENSO-forced signals depends not only on the amplitude of tropical diabatic heating but also on the amplification of its teleconnection, which is closely linked to regional atmospheric instability.

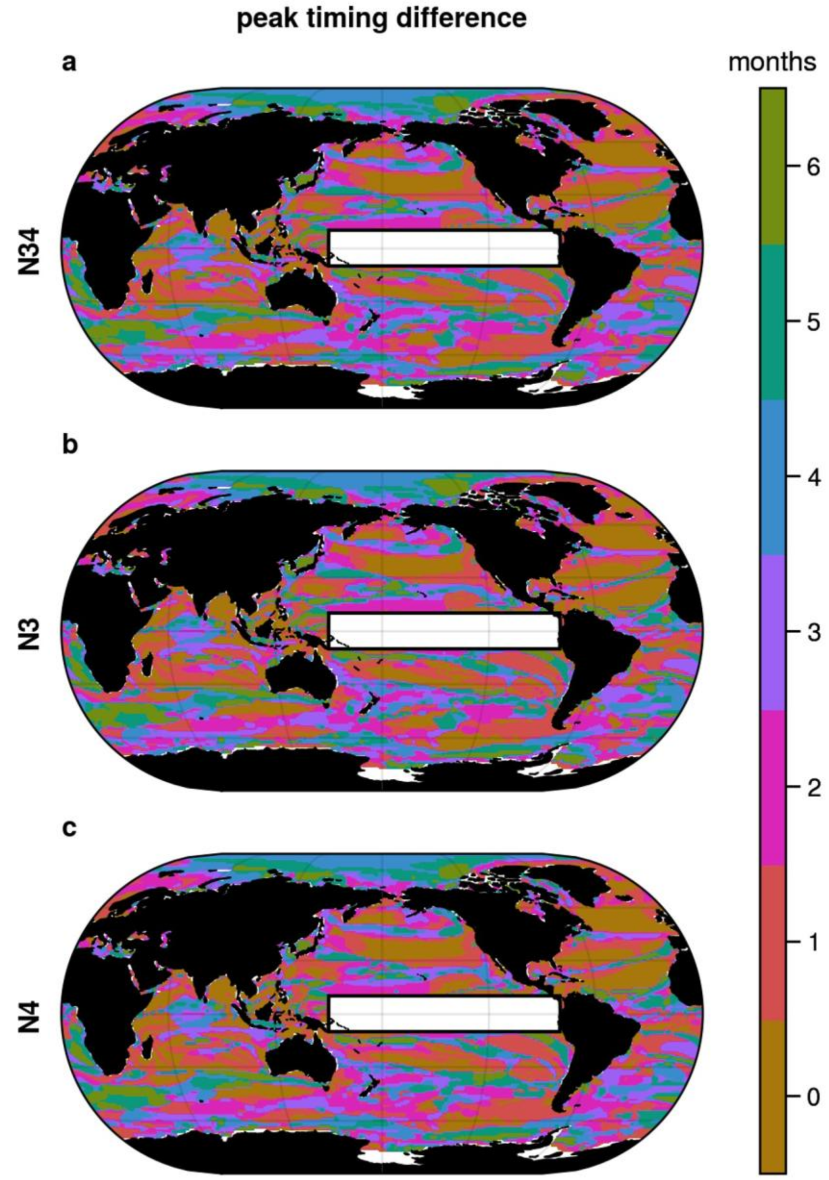

Fig. R2-1 | Peak timing difference between wind speed teleconnection peak and climatological wind-variance maximum. a-c show global maps of the minimum cyclic difference (0-6 months) between (i) the peak timing of wind-speed regressed on **a** Niño3.4, **b** Niño3 and **c** Niño4 and (ii) the timing of the climatological wind variance maximum at each grid point. Difference are computed on a 12-month cycle so that adjacent months across the year boundary are treated as close in time. The ENSO reference region (white box) are excluded.

In the response to my Comment 2, the authors state that the pattern correlation between the *climatological mixed layer depth (MLD) and the peak R2 was sufficiently small. However, are you not including the tropical Pacific in the correlation calculation? As the authors mentioned in another section, the auto-correlation in the tropical Pacific should be excluded from the analysis. Please check whether a significant negative correlation appears outside the tropical Pacific.*

Ans) In our previous response, the pattern correlations between the climatological mixed layer depth (MLD) and the peak R^2 were already computed after masking out the tropical Pacific, in line with our statement that the strong autocorrelation in the tropical Pacific should not be used for this diagnostic. Specifically, in both the previous and current analyses, grid points within 10°S–10°N and 150°E–80°W were excluded before calculating the pattern correlations.

With this masking applied, the pattern correlation between present-day (PD) climatological MLD and the peak R^2 is r = –0.05, and the correlation between PD climatological MLD and the change in peak R^2 is r = 0.02. Both values are very small and statistically insignificant, indicating that regions with large peak R^2 or enhanced peak R^2 under warming are not systematically co-located with shallow MLD outside the tropical Pacific.

Would there not also be a meaningful correlation between the changes in MLD under global warming and the corresponding changes in peak R2? I encourage the authors to examine this relationship carefully.

Ans) To address the reviewer's suggestion, we examined the relationship between changes in climatological MLD under global warming and the corresponding changes in peak R^2. We computed the area-weighted pattern correlation between the change in climatological MLD (future minus present-day) and the change in peak R^2, again masking out the tropical Pacific (10°S–10°N, 150°E–80°W) to avoid the effect of strong local autocorrelation there. The resulting correlation is r = 0.03, which is small and not statistically significant. This confirms that regions where peak R^2 increases under warming are not systematically collocated with regions of MLD shoaling or deepening, supporting our conclusion that MLD changes play at most a secondary role in organizing the pattern of enhanced ENSO-induced SST variability.

In addition, please check whether the responses to tropical forcings in the Atlantic and Indian Ocean basins show similar behavior. I believe it is important to carefully consider whether the logical development of the paper should start specifically from ENSO, or rather from tropical forcing more broadly.

Ans) Thanks again for the constructive comments. As we pointed out in the previous response, we fully agree with the reviewer that the underlying mechanism is not strictly unique to ENSO and may operate more generally for other tropical modes. To address this point more directly, we have carried out new partial linear regression analyses using Indian Ocean and tropical Atlantic indices. In these calculations, we use the Dipole Mode Index to represent tropical Indian Ocean variability (DMI; Saji et al., 1999) and the Atlantic 3 Index (ATL3; 20°W–0°, 2.5°S–2.5°N; Zebiak, 1993 and Hu et al., 2022) to represent tropical Atlantic variability, taking SON as the mature season for DMI and JJA as the mature season for ATL3. We form 3-month seasonal means of SST anomalies and of each index, and for each basin we construct a ±3-month lag window around its mature season (i.e. seven 3-month seasons; from JJA(0) to D(0)JF(1) for DMI and from MAM(0) to SON(0) for ATL3). We then compute partial linear regressions of the SST anomalies onto each basin index while statistically removing ENSO-related variability by including the Niño3.4 index as a control variable. For each grid point and each basin, we evaluate the partial correlation and corresponding regression coefficient at all seven lags, define the "peak" response as the lag at which the absolute partial correlation is maximized, and compare the present and warming climates in terms of the change in this peak partial regression amplitude.

These new results show that, even after removing ENSO, both the Indian Ocean and tropical Atlantic modes exhibit an increase in their remote SST influence under warming: the SST responses increase from the present to the warming climate for each tropical mode (Fig. R2-2). These results support the reviewer's view that the mechanism we highlight is not confined to ENSO alone but can also operate for other tropical forcings (modes).

At the same time, ENSO remains the dominant contributor to global SST variability. The SST responses per 1 standard deviation Niño3.4 are substantially larger than the corresponding DMI or ATL3 responses in both climates, and the increase under warming is also largest for Niño3.4. In the CMIP6 multi model mean, the change in SST responses is approximately 0.097 K for Niño3.4, compared to 0.060 K for DMI and 0.055 K for ATL3. Accordingly, while the same mechanism can apply across tropical basins, the IOD and ATL3 effects remain clearly secondary to ENSO in terms of the magnitude of their global teleconnection influence. Thus, as we outlined in our previous response, our primary goal in this study is to clarify the ENSO pathway because ENSO remains the strongest, most spatially extensive, and most recurrent driver of interannual tropical–global SST variability, whereas Indian and Atlantic modes typically exhibit weaker, more regionally confined, and less model-robust teleconnections. For this reason, we would like to keep focus on the ENSO impacts, but we explicitly discussed this broader interpretation in the Discussion section by adding a new paragraph.

(L251-262): Although our analysis focuses on ENSO, the mechanisms we identify are not exclusive to ENSO and are likely relevant to tropical SST forcing more generally. To test this, we performed additional partial linear regression analyses using indices for the Indian Ocean and the tropical Atlantic, after statistically removing ENSO-related variability. The results show that these modes also display a strengthened influence on remote SSTs under warming (Supplementary Fig. 17). This consistency supports our interpretation that the amplification of ENSO impacts mainly results from (i) stronger diabatic heating and the associated atmospheric teleconnections, and (ii) a larger air–sea specific humidity contrast—processes that can likewise operate for other tropical SST forcings. A more comprehensive assessment is, however, needed to fully quantify the enhanced impacts of non-ENSO tropical modes, which we leave for future work.

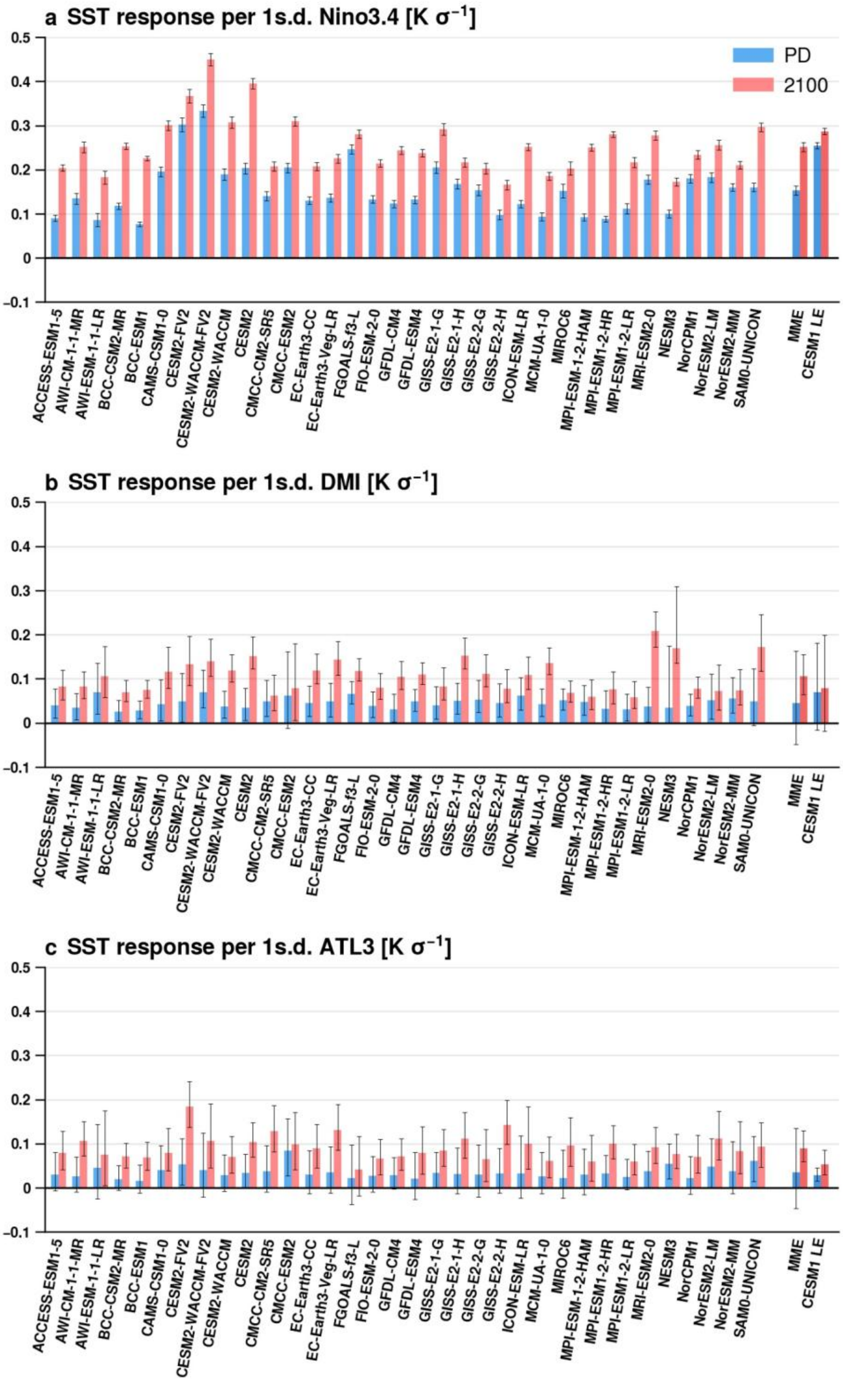

Fig. R2-2 | Strengthening of SST response to tropical variability modes under warming. **a** Same as Supplementary Fig.2a but for response to 1 standard deviation of Niño3.4. **b** Indian Ocean Dipole effect, defined as the difference between the future (2100) and present-day (PD) climates in the global mean absolute partial regression coefficient of SST anomalies onto the standardized Dipole mode index (DMI) at the lag of maximum partial correlation (from JJA(0) to D(0)JF(1)), after statistically removing ENSO variability with the Niño3.4 as a control variable. **c** Same as b but for the tropical Atlantic, using the ATL3 index (20°W–0°, 2.5°S–2.5°N). For each 34 CMIP6 model, multi-model mean (MME) and CESM1.

Saji, N. H., Goswami, B. N., Vinayachandran, P. N. & Yamagata, T. A dipole mode in the tropical Indian Ocean. *Nature* **401**, 360–363 (1999).

Zebiak, S. E. Air-Sea Interaction in the Equatorial Atlantic Region. *Journal of Climate* **6**, 1567-1586 (1993).

Hu, Z.-Z. et al., Global Ocean Monitoring and Prediction at NOAA Climate Prediction Center: 15 Years of Operations. *Bulletin of the American Meteorological Society 103*, E2701-E2718 (2022).

Response to Reviewer #4

I appreciate the authors' diligent effort in revising this manuscript and providing a point-by-point response. My previous major comments have been satisfactorily addressed. However, I guess a minor point need to be addressed to finalize the paper.

Comments:

1: I appreciate the significant effort and thoroughness in revising the manuscript. The addition of the quantitative decomposition analysis, separating the ENSO impact on global SST into non-amplitude and amplitude components, is a substantial and excellent improvement that greatly strengthens the rigor of your conclusions. However, the changes in ENSO amplitude remain unclear for the CESM1 and CMIP6 runs in this study. As the authors stated in the revised manuscript, ENSO amplitude changes should not be negligible, even though the non-amplitude component of ENSO plays a more significant role in influencing global SST.

Ans) We agree that ENSO amplitude changes are not negligible and can directly affect remote SST responses. To clarify this point, we revised the Discussion to explicitly state that ENSO teleconnections are proportional to the strength of tropical ENSO forcing, so an increase (decrease) in ENSO amplitude would be expected to amplify (dampen) the remote SST response, all else equal. We also clarified that ENSO amplitude changes are not robustly consistent across CESM1 and CMIP6, with the sign and magnitude varying across models and metrics, implying substantial uncertainty in the amplitude contribution.

(L236-250) : Though our study focused on changes in the SST sensitivity to ENSO, the actual ENSO impacts will also depend on changes in ENSO amplitude itself. Importantly, changes in ENSO amplitude are not clearly consistent across CESM1 and CMIP6 models, with the sign and magnitude varying across models. Because ENSO teleconnections tend to increase with the strength of tropical forcing, an increase (decrease) in ENSO amplitude would be expected to amplify (dampen) the remote SST response. To quantify ENSO's total SST influence, we decomposed it into a non-amplitude term and an amplitude term, following regression-based approaches (Supplementary Notes). The results show that the increase is dominated by the changes in non-amplitude component—~64% in CESM1 and ~76% in the CMIP6 multi-model mean—while amplitude accounts for ~32% and ~20%, respectively; importantly, even models with reduced ENSO amplitude[54–56] show a net increase because atmospheric and oceanic sensitivity strengthens (Supplementary Figs. 15 and 16). Thus, while amplitude changes are model-dependent and introduce uncertainty in the total response, the strengthening of background-state and teleconnection sensitivity provides a more robust and consistent contribution across experiments.

Response to Reviewers #3:

I appreciate the authors' careful consideration of my comments. The authors have now explicitly discussed the influence of other ocean basins in the Discussion section, and I think this largely addresses my concerns. I have only one minor comment.

Comments:

In Supplementary Fig. 17, the use of partial linear regression is not fair, because it removes all variability in the Indian and Atlantic Oceans that covaries with ENSO. For a fair comparison, either (1) Supp. Fig. 17b and c should also use standard (non-partial) regression, or (2) the influences of the Indian and Atlantic Oceans should be removed from the ENSO analysis in Supp. Fig. 17a (and similarly, the influences of ENSO and the Atlantic Ocean should be removed from the Indian Ocean analysis, and likewise for the Atlantic Ocean).

If this point is revised, I believe the manuscript would be suitable for acceptance.

Ans) Thank you for this helpful suggestion. We agree that applying partial linear regression to the Indian Ocean and Atlantic indices can remove the component of their variability that covaries with ENSO, which may hinder a fair comparison with the standard ENSO regressions. Following your option (1), we performed additional calculations using standard (non-partial) linear regression for the Indian Ocean and tropical Atlantic modes and revised Supplementary Fig. 17b and c accordingly (i.e., regression of SST anomalies onto DMI and ATL3 without removing ENSO).

Figure R1 summarizes the updated results. The standard-regression patterns and their warming-induced strengthening are highly consistent with those shown in our previous analysis, indicating that our interpretation is unchanged: the remote SST responses associated with the Indian Ocean and tropical Atlantic modes also strengthen under warming, supporting our broader point that the underlying amplification mechanism can operate for tropical forcings beyond ENSO. At the same time, the DMI and ATL3 teleconnection signals remain clearly weaker than those associated with Niño3.4, so our conclusion that ENSO provides the dominant global influence on interannual SST variability is unchanged.

We have replaced Supplementary Fig. 17b and c with these standard-regression results and clarified the corresponding description in the Supplementary Information. We thank the reviewer again for this comment, which improved the methodological fairness and clarity of Supplementary Fig. 17.

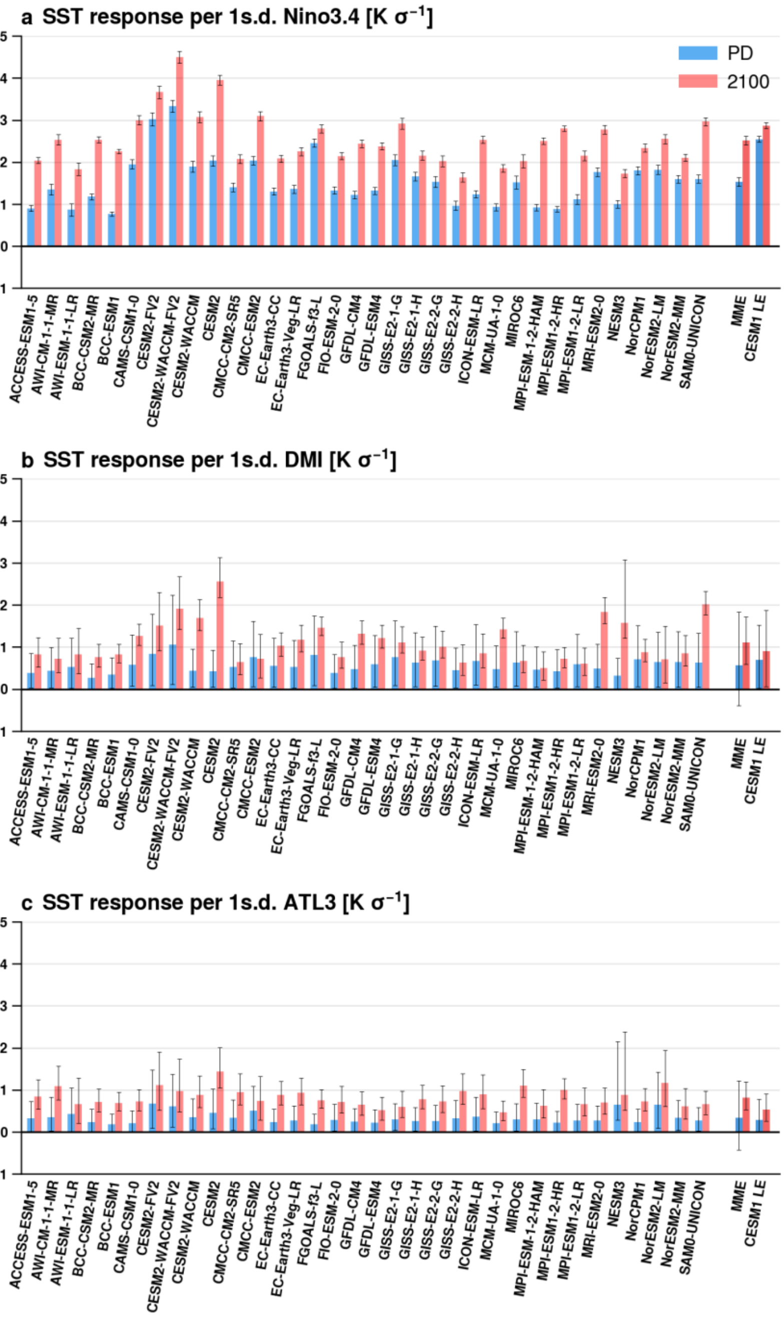

Fig. R1 | Strengthening of SST response to tropical variability modes under warming. a Same as Supplementary Fig.2a but for response to 1 standard deviation of Niño3.4. **b** Indian Ocean Dipole effect, defined as the difference between the future (2100) and present-day (PD) climates in the global mean absolute regression coefficient of SST anomalies onto the standardized Dipole mode index (DMI) at the lag of maximum correlation (from JJA(0) to D(0)JF(1)). **c** Same as b but for the tropical Atlantic, using the ATL3 index (20°W–0°, 2.5°S–2.5°N). For each 34 CMIP6 model, multi-model mean (MME) and CESM1.